

1 Manuscript type: Research article

2 **COMPREHENSIVE LANDSLIDE SUSCEPTIBILITY MAP OF CENTRAL ASIA**

3 Ascanio Rosi^{a,b}, William Frodella^{b,c,*}, Nicola Nocentini^{b,c}, Francesco Caleca^{b,c}, Hans Balder Havenith^d, Alexander
4 Strom^{e,f}, [Mirzo Saidov^g](#), [Gany Amirgalievich Bimurzaev^h](#), Veronica Tofani^{b,c}

5 ^a Department of Geosciences, University of Padua, Via G. Gradenigo 6, 35131, Padua, Italy

6 ^b UNESCO Chair on the Prevention and Sustainable Management of Geo-Hydrological Hazards, University of
7 Florence, Largo Fermi 2, 50125 Florence, Italy

8 ^c University of Florence, Department of Earth Sciences, via G. la Pira 4, 50121 Florence, Italy.

9 ^d Department of Geology, University of Liege, 4000 Liege, Belgium

10 ^e Geodynamics Research Center LLC, Moscow, 125008, Russian Federation

11 ^f Geodynamics Research Center - branch of JSC “Hydroproject Institute”, Moscow, 125993, Russian Federation

12 ^g [Institute of Water problems, Hydropower, Engineering and Ecology of Tajikistan \(IWPHE\), 734063, Dushanbe,](#)
13 [Tajikistan](#)

14 ^h [State Service of the Republic of Uzbekistan for Geohazards Monitoring, 100074, Tashkent, Uzbekistan](#)

15 * Correspondence: william.frodella@unifi.it; +39 055 2755979

16 **Abstract**

17 Central Asia is an area characterized by complex tectonics and active deformation; the related seismic activity
18 controls the earthquake hazard level that, due to the occurrence of secondary and tertiary effects, has also direct
19 implications on the hazard related to mass movements as landslides, which are responsible for an extensive number
20 of casualties every year. Climatically, this region is characterized by strong rainfall gradient contrasts, due to the
21 diversity of climate and vegetation zones. The region is drained by large, partly snow- and glacier-fed rivers, that
22 cross or terminate in arid forelands; therefore, it is affected also by a significant river flood hazard, mainly in spring
23 and summer seasons. The challenge posed by the combination of different hazards can only be tackled considering
24 a multi-hazard approach harmonized among the different countries, in agreement with the requirements of the
25 Sendai Framework for Disaster Risk Reduction. This work was carried out within the framework of the SFRARR
26 Project (“*Strengthening Financial Resilience and Accelerating Risk Reduction in Central Asia*”) as a part of a
27 multi-hazard approach, and is focused on the first landslide susceptibility analysis at a regional scale for Central
28 Asia. To this aim the most detailed landslide inventories, covering both national and transboundary territories were
29 implemented in a Random Forest model, together with several independent variables. The proposed approach
30 represents an innovation in terms of resolution (from 30 to 70 m) and extension of the analysed area with respect
31 to previous regional landslide susceptibility and hazard zonation models applied in Central Asia. The final aim
32 was to provide a useful tool for land use-planning and risk reduction strategies to landslide scientists, practitioners,
33 and administrators.

34 **1. Introduction**

60 During the two decades spanning between 1988 and 2007, according to observed estimates, out of 177 reported
 61 disasters in Central Asia 13% were landslides, causing 700 deaths ([Table 1](#)), while in the same period
 62 economic losses have been as high as \$150 million, including damage to infrastructures, settlements and
 63 agricultural/pasture lands, as well as displacement of the population (GFDRR, 2009). More recent modelled
 64 estimates show that in the Central Asia states an annual average of 3 million persons are affected by earthquakes
 65 and floods, with an estimated annual average GDP of 9 billion USD (GFDRR, 2016).

66 **Table 1: Observed landslide hazard statistics (1988-2007).** Source: Risk assessment for Central Asia and
 67 Caucasus (UN ISDR, 2009).

Country	No. disasters/year	Total no. of deaths	Deaths/year	Relative vulnerability (deaths/year/million)
Kazakhstan	0.05	48	2.40	0.16
Kyrgyz Republic	0.30	238	11.90	2.27
Tajikistan	0.50	339	16.95	2.51
Turkmenistan	n.a.	n.a.	n.a.	n.a.
Uzbekistan	0.15	75	3.75	0.14

68
 69 Due to their large size and impact, most of the occurring landslides have profound transboundary implications.
 70 Tajikistan and Kyrgyz Republic are the countries most impacted by landslides: in Tajikistan around 50000
 71 landslide were mapped, 1,200 of which threaten settlements or facilities (Thurman, 2011), while Kyrgyz Republic
 72 has been affected by 5,000 landslides, of which 3,500 at various levels of activity are located in the southern
 73 portion of the country (the Fergana Valley area) (Pusch, 2004; Li et al., 2021). Only in Kyrgyz Republic, up to
 74 2017, 784 landslides and 1658 mudflows (also including loess flows) and flash floods caused 352 victims
 75 (Kalmetieva et al., 2009; Havenith et al., 2015a; 2017). Almaty province in Kazakhstan, Tashkent, Samarkand,
 76 Surkhandarya, Kashkadarya Provinces of Uzbekistan, and Ahal Province of Turkmenistan are also exposed to
 77 landslides (World Bank, 2006). Given the increased anthropogenic pressures and the impact of climate change,
 78 since the early '90s several projects have tried to improve the knowledge on landslide hazard (Thurman, 2011),
 79 by providing landslide losses estimations, location, type, triggering/reactivation dates, inventories and hazard/risk
 80 maps, as well as platforms to retrieve open disaster risk data and overviews on landslide risk reduction strategies.
 81 Amongst the regional studies on landslide hazard, providing descriptions, statistics, and inventory maps, it is worth
 82 mentioning:

- 83 • Disaster Risk Management and Climate Change Adaptation in Europe and Central Asia, developed by the
 84 World Bank - Global Facility for Disaster Reduction and Recovery (Pollner et al., 2010).

- 85 • Disaster Risk Reduction, 20 Examples of Good Practice from Central Asia, developed by the European Union,
86 International Strategy for Disaster Reduction ISDR (European Commission Humanitarian Aid, Civil
87 Protection, 2006).
- 88 • Science for Peace Project (983289) ‘Prevention of landslide dam disasters in the Tien Shan, LADATSHA’.
89 2009–2012, NATO Emerging Security Challenges Division.
- 90 • PROGRESS (Potsdam Research Cluster for Georisk Analysis, Environmental Change and Sustainability).
91 German Federal Ministry of Research and Technology (BMBF).
- 92 • Tian Shan-Pamir Monitoring Program (TIPTIMON). German Federal Ministry of Education and Research
93 (BMBF).
- 94 • M126 IPL Project (funded by the International Consortium on Landslides): M2002111 Detailed study of the
95 internal structure of large rockslide dams in the Tien Shan; M2004126 Compilation of landslide/rockslide
96 inventory of the Tien Shan Mountain System.

97 Besides the creation of landslide inventories, a common approach to assess landslide hazard is the development of
98 landslide susceptibility maps (LSMs), which depict the relative probability of occurrence of a given type of
99 landslide in a given area, without considering the probability of occurrence in time (Brabb, 1984). In other words,
100 LSMs identify those areas where landslides can occur, based on their geological, morphological, and climatic
101 characteristics. These maps have been extensively used as useful tools for land planning (Cascini 2008; Frattini et
102 al., 2010) and hazard assessment (Corominas et al., 2003). More recently, they have been successfully integrated
103 also in quantitative risk assessment (Chen et al., 2016), and early warning systems (Segoni et al., 2018; Tiranti et
104 al., 2019). LSMs have been produced by applying a wide range of mathematical techniques, from the most
105 traditional statistic approaches like frequency ratio (Yilmaz, 2009), discriminant analysis (Carrara, 1983; Trigila
106 et al., 2013) and logistic regression (Lee, 2005; Duman et al., 2006; Manzo et al., 2013), to more recent and more
107 advanced techniques, like artificial neural network (Tien Bui et al., 2016; Ermini et al., 2005), machine learning
108 (Catani et al., 2013) and multi criteria decision analysis (Akgun, 2012). Statistical-probabilistic models for
109 landslide susceptibility can overcome the data gaps and allow to analyse very wide areas (from basin to national
110 scales), by adopting a homogeneous methodology and a harmonized dataset (including global and local data
111 sources). However, landslide hazard assessment is a complex process since it needs accurate knowledge of the
112 topic and appropriate input data (historical inventories, and regional inventories that consist of large prehistoric
113 events mainly). In this work the landslide susceptibility analysis was carried out by means of the “Random Forest”
114 machine learning algorithm, which is credited as one of the most advanced and reliable techniques in this field
115 (Catani et al., 2013, Goetz et al 2015). This work represents the first landslide susceptibility analysis at a regional
116 scale for Central Asia, and was carried out in the framework of the SFRARR Project (“Strengthening Financial
117 Resilience and Accelerating Risk Reduction in Central Asia”) as a part of a multi-hazard approach (Bazzurro et
118 al., in prep). The main challenge of this work was the creation of a unique LSM of the whole Central Asia, that
119 involved the use of a wide range of variables, to account the features of each country, a high volume of input data,
120 and the development of new approaches to analyse these data and to take into accounts possible discrepancies and
121 non-homogeneities. The proposed approach represents an innovation in terms of resolution, extension of the
122 analysed area with respect to previous regional landslide susceptibility and hazard zonation models applied in

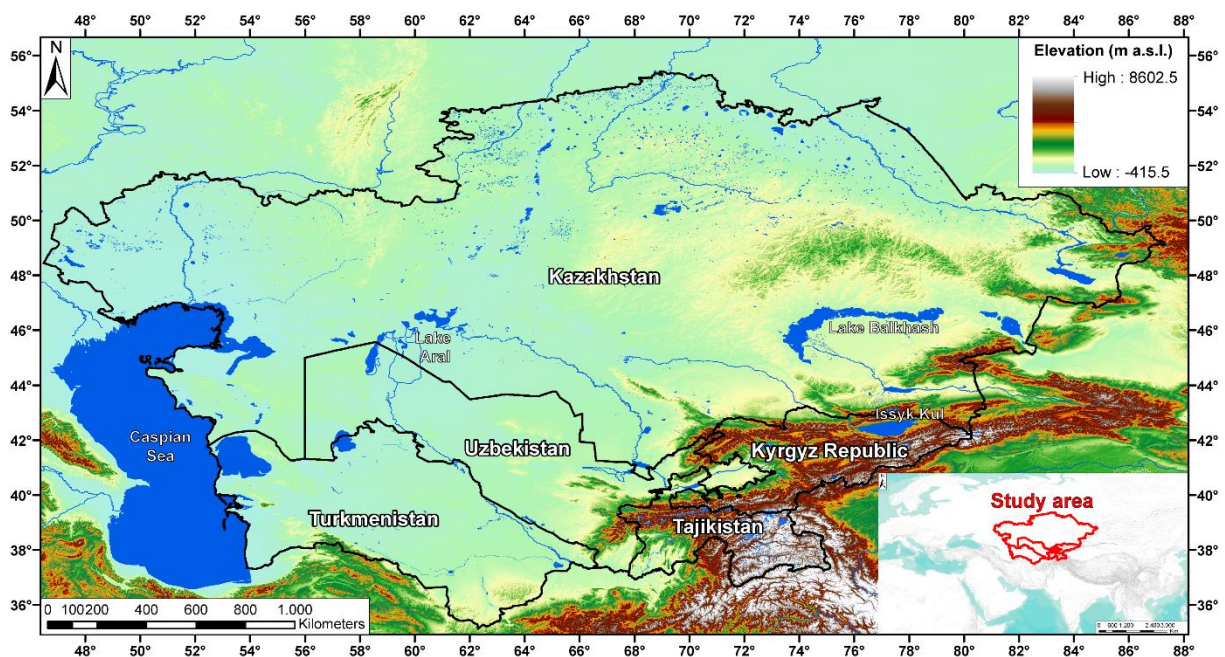
123 Central Asia (e.g., Nadim et al., 2006; Havenith et al., 2015b; Stanley and Kirshbaum, 2017; Pittore et al., 2018;
124 World Bank, 2020). ~~For the studied area the landslide susceptibility distribution in the area covered by elements~~
125 ~~at risk, such as roads, railways, and buildings, was also assessed (Scaini et al., in prep).~~

126

127 2. Study area

128 Geographically, Central Asia is a vast and diverse region including high mountain chains, deserts, and steppes
129 (Fig. 1). A large portion of the Central Asia countries, especially the southern and eastern parts of the region, are
130 occupied by the mountainous areas of the Djungaria, Tien Shan, Pamir, Kopetdag, and small part of Western Altaj,
131 with peaks above 7,000 m a.s.l (Strom, 2010). These intraplate mountain systems formed in the Cenozoic between
132 the Tarim Basin and the Kazakh Shield, as a result of the India-Asian collision (Molnar and Tapponier 1975,
133 Abdrakhmatov et al., 1996; 2003; Zubovich et al., 2010, Ullah et al., 2015). This work is focused in the most inner
134 part of Central Asia, represented by the territories of Turkmenistan, Kazakhstan, Kyrgyz Republic, Uzbekistan,
135 and Tajikistan. Active mountain building started in the Oligocene (Chedia 1980) or even later (Abdrakhmatov et
136 al. 1996), forming a complex system of basement folds disrupted by numerous thrusts and reverse faults with
137 significant amount of lateral offset (Delvaux et al. 2001). Several regional fault zones are aligned along large parts
138 of the mountain belts, others cross the orogen in a NW-SE direction, e.g., the Talas-Fergana fault, which forms a
139 distinct boundary between the western and central Tien Shan (Trifonov et al. 1992) (Fig. 2).

140

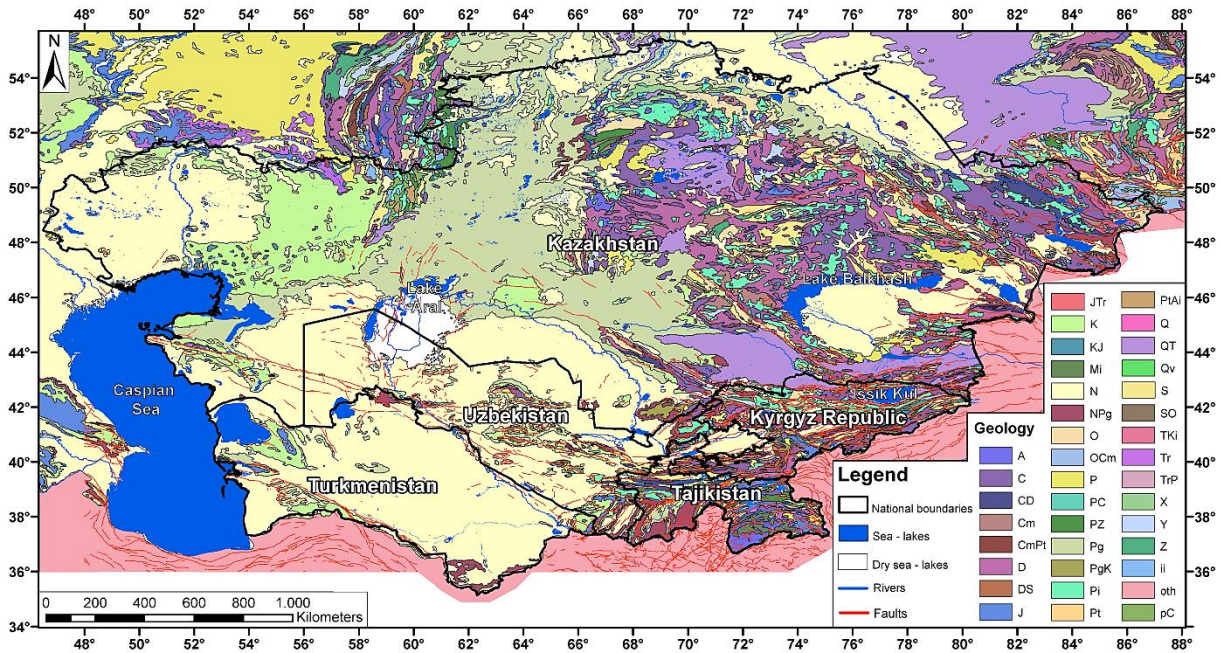


141 **Figure 1. Study area geographical-geomorphological setting.** Lakes' polygons from Schiavina et al., 2022,
142 while MERIT DEM (Yamazaki et al. 2017) was used as topographic base.

143 Mountain ridges, formed mainly by palaeozoic crystalline rocks, are separated by wide lenticular or narrow, linear
144 intermountain depressions, containing Neogene and Quaternary deposits, mainly sandstone, siltstone with gypsum
145 interbeds, and conglomerates (Strom and Abdrakhmatov, 2017). Mesozoic and Paleogene deposits are typical of

146 the foothill areas. Almost every ridge, especially in the Tien Shan, corresponds to a neotectonic anticline, and most
 147 of the main river valleys follow intermontane tectonic depressions, which are linked by narrow deep gorges up to
 148 1-2 km deep (Strom and Abdrakhmatov, 2018). These mountain systems are the sources of most of Central Asia
 149 rivers, which, being fed by glaciers, snowmelt water and rain, have deeply incised valleys.

150 Such extreme topography along with complex geological structure, active tectonics and high seismicity determine
 151 important landslide predisposing factors, making landslides the third most prevalent natural hazard in Central Asia,
 152 following earthquakes and floods (CAC DRMI, 2009; Havenit et al, 2017).



153
 154 **Figure 2. Geological map of the study area.** Geological formation data from United States Geological Survey
 155 (see Persits et al., 1997 for the legend), including faults from the AFEAD (Active Faults of Eurasia) database
 156 (Styron and Pagani, 2020).

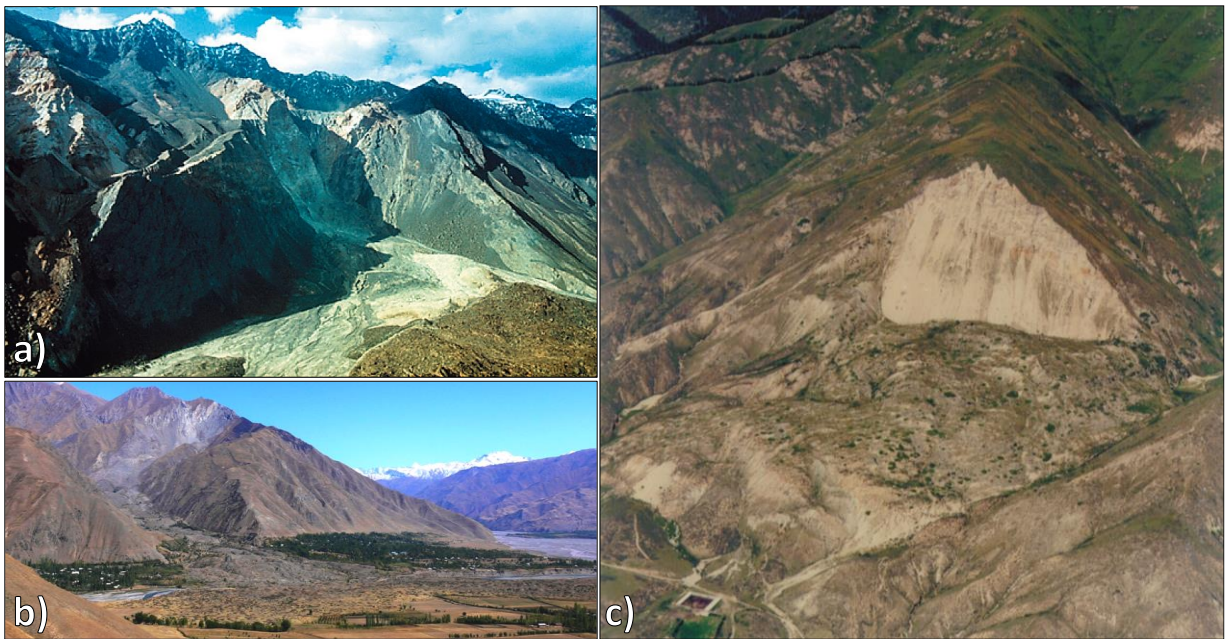
157 **2.1 Landslide types in Central Asia**

158 According to the international Cruden and Varnes 1996 classification, landslides phenomena in Central Asia
 159 include rockslides/rock avalanches, rotational/translational slides and mud/debris flows (often involving loess),
 160 which are triggered by natural events such as earthquakes, floods, rainfall and snowmelt (Behling et al., 2014;
 161 2016; Golovko, 2015; Havenith et al., 2006a,b, 2015a, b; Kalmetieva et al., 2009; Saponaro et al., 2014; 2015;
 162 Strom and Abdrakhmatov, 2017; 2018). Glacial lakes outburst flood phenomena, caused by the breach of natural
 163 glacial dams, often result in large scale catastrophic mud/debris flows. In Central Asia, landslides more often occur
 164 in the loess zone of contact with other rocks, on clay interlayers of the Mesozoic and Cenozoic age, reaching a
 165 volume from tens of thousands up to $15-40 \cdot 10^6 \text{m}^3$ (Juliev et al., 2017). Seismically triggered landslides are very
 166 common in tectonically active mountain regions, such as Tien Shan and Pamir (Sternberg et al., 2006; Hong et al.,
 167 2007; Juliev et al., 2017). According to the literature background, most of the large mapped mass movements
 168 (especially those with a volume of more than 10^6m^3) were triggered generally by major (also prehistoric)
 169 earthquakes, possibly in combination with climatic factors, namely snowmelt and heavy rainfall (Havenith et al.,

170 2003; Strom and Korup, 2006; Strom, 2010; Schlögel et al., 2011; Strom and Abdrakhmatov 2017, 2018; Havenith
171 et al., 2015a; 2016; Behling et al., 2014; 2016; Piroton et al., 2020). Furthermore, in the past few decades, the
172 number and intensity of landslides have grown owing to climate change and the increase of the anthropic pressure,
173 due to several factors such as the uncontrolled land and water use, the rising of the water tables (often induced by
174 the increase of irrigation; Ishihara et al., 1990), mining, and excavation activities (Pollner et al., 2010; Thurman,
175 2011).

176 **2.2 Large Rockslides and natural dams**

177 Numerous rockslides have occurred in the mountains producing hazardous natural phenomena such as long runout
178 rock avalanches (Fig. 3) and dammed lakes, more than 100 of which still store water (Strom, 2010). These mainly
179 involve the Palaeozoic magmatic and metamorphic crystalline bedrock, but also the sandstone and limestone
180 formations. Although according to Strom, 2010, many of the existing dammed lakes should be considered as stable,
181 catastrophic outburst floods that occurred in the 20th century, emphasize high potential hazard of landslide natural
182 blockages. Havenith et al., 2015a report a catalogue of large to giant landslides (having volumes exceeding $>10^7$
183 m^3) in the Tien Shan area, showing several information such as location, time of occurrence, volumes, and
184 thickness. Regarding the volumes of these rockslides, these range from $50 \cdot 10^3 m^3$ to $10 km^3$ (Strom and Korup,
185 2006; Strom and Abdrakhmatov, 2018). Many of these phenomena, though not all, were triggered by earthquakes
186 with $M > 6$ and have dammed a river valley (some of the dams have been naturally or artificially breached).



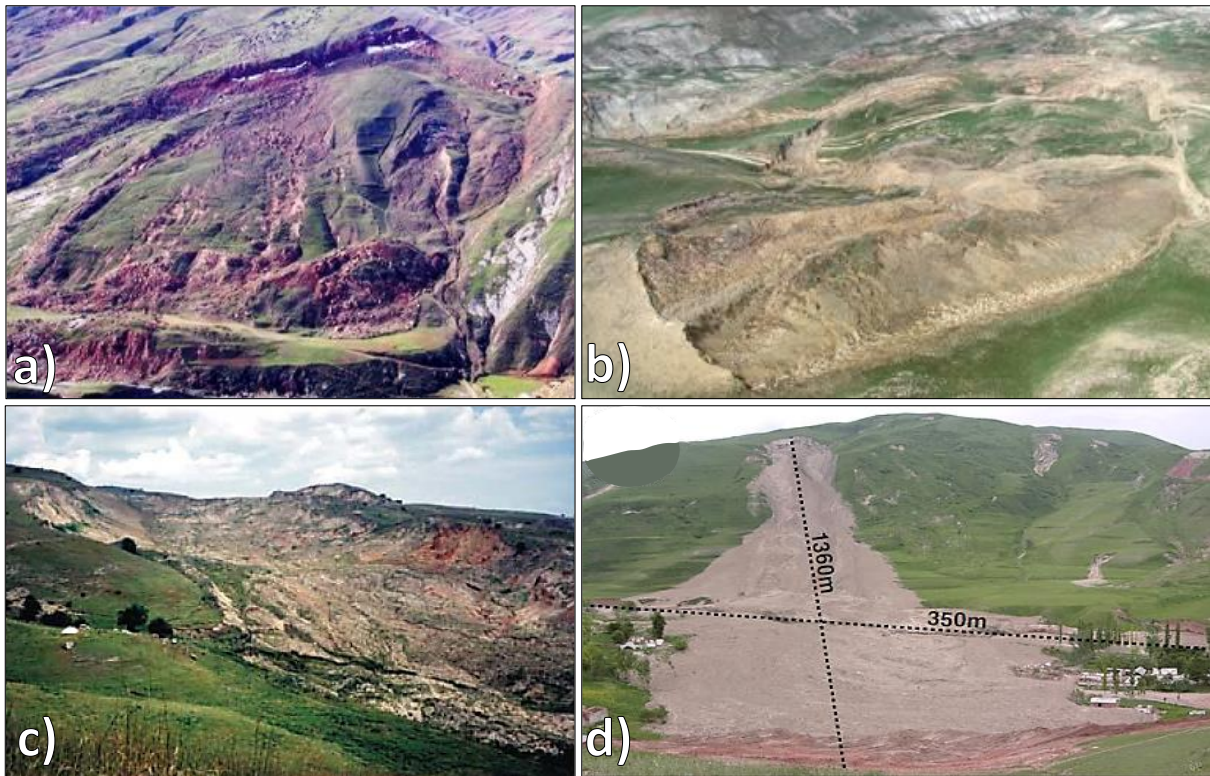
187
188 **Figure 3. Examples of large rockslide features in Central Asia.** Helicopter view of the Usoi landslide scarp,
189 triggered by the 1911 earthquake, Tajikistan (a) (after Strom, 2010); Khait rock avalanche (b) (after Havenith et
190 al., 2015a); helicopter view of Ananevo landslides (c) (after Havenith et al., 2015a).

191 **2.3. Landslide in soft rocks and loose deposits**

192 Rotational landslides mostly occur in loose unconsolidated Quaternary deposits, and in soft and semi-hard rock
193 layers in Mesozoic-Cenozoic sediments, represented mainly by layers of clays, claystones, siltstones, sandstones,

194 marls, limestone, gypsum, and conglomerates, with intercalated clays (Roessner et al., 2004; Kalmatieva et al.,
195 2009) (Fig. 4). These phenomena can create river dams, but they rarely are long-living dams, since usually they
196 are small and their bodies are eroded quickly even if they block a river channel (Strom and Korup, 2006).

197 The loess landslides occur quite regularly (on a yearly basis) in the regions presenting an almost continuous and
198 locally very thick (>20 m) cover of this material, generally at mid-mountain altitude (900— 2,300 m) and mainly
199 along the border of the Fergana Basin (Kyrgyz Republic, Uzbekistan, and Tajikistan), and on the southern border
200 of the Tien Shan in Tajikistan (Fig. 4).



201
202 **Figure 4. Examples of landslides in soft rocks-loose deposits.** Picture the Kamar landslide (a) and the Beshbulak
203 landslide (b) (after Niyazov and Nurtaev, 2013). Examples of loess slides and mixed loess—soft landslides in NE
204 Fergana valley: Kochkor-Ata landslide failure in spring 1994 (c) (after Roessner et al., 2005); Field photo of the
205 Kainama landslide (d) (after Behling et al., 2016).

206 Loess flow landslides and debris flows, involving the eluvial slope cover, represent a relevant hazardous
207 phenomenon in the mountainous regions of Kazakhstan, in the area of Almaty, near the southern border with
208 Kyrgyz Republic, in the Altai area (Medeu and Blagovechshenskiy, 2016), around the Fergana Basin, all along
209 the border between Tajikistan and Kyrgyz Republic and around the Tajik Depression. Landslides occurring in
210 Quaternary loess units of up to 50 meters thick are characterized by very rapid avalanche-like mass movements,
211 which can reach several meters per second (often represent a combination of rotational slide and dry flow resulting
212 in long runout zones; World Bank, 2008). Typically, pure loess landslides have a volume of hundreds up to one
213 million cubic meters and appear as clusters (Roessner et al., 2005). From the recent history it appears that pure (or
214 quasi-pure) loess slides and flows are particularly dangerous because of their high velocity and long runout which,

215 in turn, can generate a great destructive power and more severe disasters than other types of mass movements of
216 similar size (Havenith et al., 2015a; Behling et al., 2014; 2016). If failure also affects underlying materials (mostly
217 Mesozoic and Cenozoic soft rocks), the volume of these mixed slides can exceed $10 \times 10^6 \text{ m}^3$.

218 These kinds of landslides are particularly deadly and can be triggered by a combination of long-term slope
219 destabilization factors (e.g., rainfall and snowmelt) and short-term triggers (e.g., seismic shocks). Even though
220 earthquake-triggered loess slides and flows are far less frequent than rainfall triggered ones, they caused much
221 larger disasters in recent history, such as those triggered, respectively, by the July 1949 Khait and the January 1989
222 Gissar earthquakes. The number of active debris flow basins in Kazakhstan is over 300 with registered cases of
223 more than 600 debris flows of different genesis (80% of which are represented by heavy rainfall-triggered debris
224 flows, while the glacial debris flows make up about 15% of the total) (Yaning, C., 1992).

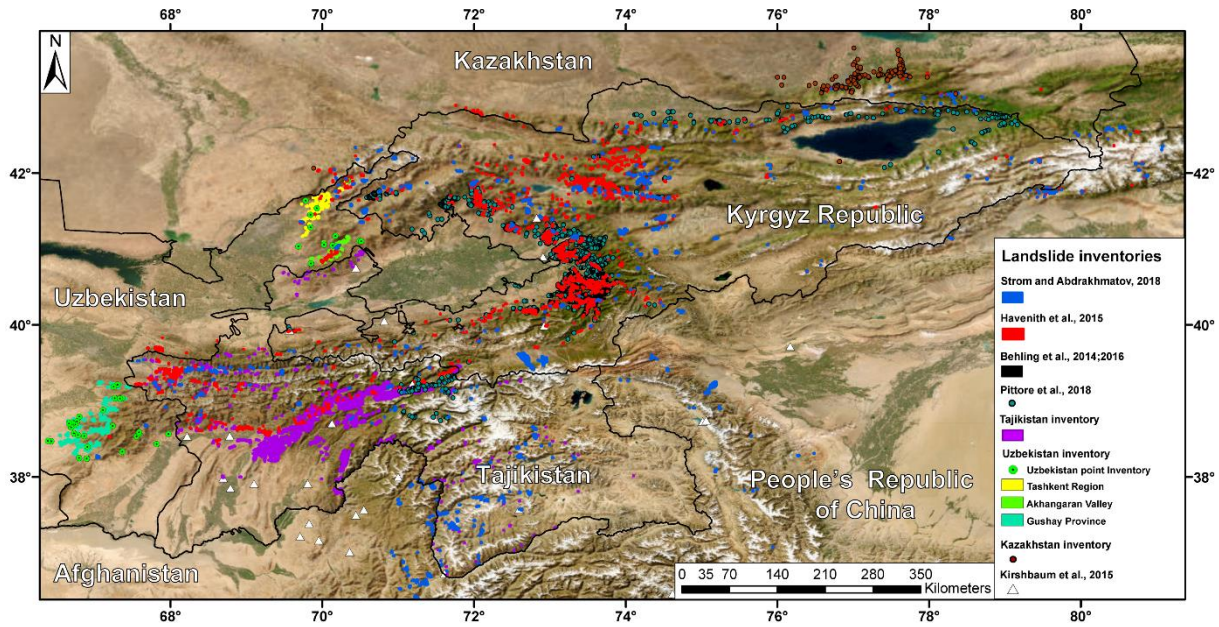
225 **3 Materials and Methods**

226 *3.1 Landslide databases*

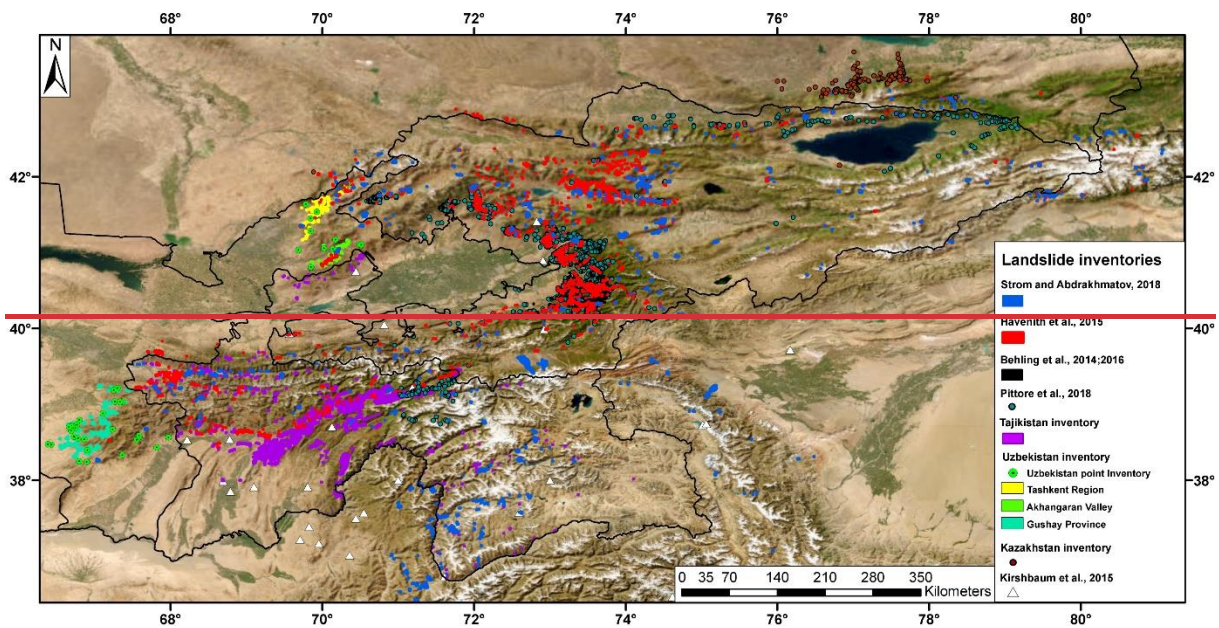
227 To implement the adopted susceptibility models the largest, most accurate, and updated landslide inventories were
228 used (Fig. 5). These were compiled by several authors by means of decades of field surveys, remote sensing and
229 geophysical analysis in the study area.

230 Hereafter we report their description in detail (Tab. 2):

- 231 • The “Tien Shan landslide inventory” (Havenith et al., 2015a): represents the largest inventory in the study
232 area. Compiled by means of field surveys, remote sensing data interpretation and geophysical surveys, it
233 comprises the rockslides of the previous inventory together with other smaller landslides in soft sediments
234 (Havenith et al. 2006a; Schlögel et al., 2011) for a total of 3,462 landslides polygons, also including
235 information on landslide length and area.
- 236 • The “Rockslides and Rock Avalanches of Central Asia” (Strom and Abdrakhmatov, 2018): a large inventory
237 including ~~860~~^{over 1000} polygons of large-scale ($\geq 1 \text{ Mm}^3$) rockslides and rock avalanches, covering central
238 Asian countries (except for Turkmenistan and Altai) plus Chinese Tien Shan and Pamir, and Afghan
239 Badakhshan. Compiled in decades of field work and analysis of aerial/satellite imaging, it also comprises
240 information on landslide morphometric parameters (runout, area), and 126 polygons on possible landslide
241 bodies, dammed lakes, and head-scarps. Quantitative characteristics (area, volume, runout, etc.) for about 600
242 cases are provided as well.



243



244

245 **Figure 5. Map of the adopted landslide inventory maps.** Basemap source: Esri, Maxar, Earthstar Geographics,
 246 and the GIS User Community.

247 ~~• The “Tien Shan landslide inventory” (Havenith et al., 2015a): represents the largest inventory in the study~~
 248 ~~area. Compiled by means of field surveys, remote sensing data interpretation and geophysical surveys, it~~
 249 ~~comprises the rockslides of the previous inventory together with other smaller landslides in soft sediments~~
 250 ~~(Havenith et al. 2006a; Schlögel et al., 2011) for a total of 3,462 landslides polygons, also including~~
 251 ~~information on landslide length and area.~~

252 • The “Multi-temporal landslide inventory for a study area in Southern Kyrgyz Republic derived from RapidEye
 253 satellite time series data (2009 – 2013)” (Behling et al., 2014; 2016; 2020), is a semi-automated spatiotemporal
 254 landslide inventory for the period from 1986 to 2013, covering a 2,500 km² in the Fergana valley rim in

southern Kyrgyz Republic. This inventory includes ~~2,0524,582~~ landslide polygons mapped from multi-sensor optical satellite time series data, together with information on spatiotemporal landslide activity patterns (area and year of trigger).

- “The EMCA landslide catalogue Central Asia” (Pittore et al., 2018), including 3,1~~2930~~ points, which covers mostly western and northern Kyrgyz Republic as well as Tajikistan’s Region of Republican Subordination. The catalogue is a summary (point locations) of the documented landslides between 1954 and 2009 (Kalmetieva et al., 2009), which are collected by the Central Asian Institute for Applied Geosciences through geological surveys (field campaigns) on single sites close to urban areas.
- The “Tajikistan landslide database” provided by the Institute of Water problems, Hydropower, Engineering and Ecology of Tajikistan (IWPHE), which includes 2,~~822740~~ landslide polygons and 114 landslide-prone areas (with information on length and area).
- The “Uzbekistan landslide inventory” provided by the Institute of Seismology of the Academy of Science of Uzbekistan (ISASUZ) and the State Monitoring Service of the Republic of Uzbekistan for hazardous geological processes, which covers the Tashkent ~~province~~ Gushay provinces, and the Akharangan Valley. It comprises a 49 point inventory (including location, type, volume, length, and date of triggering; Nyazov R.A. 2020) and a polygon inventory digitized for this project from the maps in Juliev et al., 2017 (including a total ~~3245~~ landslide polygons).
- The “Kazakhstan landslide inventory”, provided by the Institute of Seismology Limited Liability Partnership (LLP) LLP “Institute of Seismology” of the Science Committee of the Republic of Kazakhstan, covering mainly the Tien Shan area at the border with Kyrgyz Republic, and small part of the western Altai, including 254 point-objects with information on type, area/volume, triggering date.
- Part of the “Global Landslide Catalogue (GLC)” (Kirshbaum et al., 2015), which covers Kyrgyz Republic and Tajikistan, including 15 landslide point with a description on landslide size/type and triggering date/factor. The GLC was compiled since 2007 at NASA Goddard Space Flight Centre NASA and considers all types of mass movements triggered by rainfall, which have been reported in the media, disaster databases, scientific reports, or other sources.

Table 2. Name of the Landslide Inventory Maps (LIM) of the study area.

<u>LIM name</u>	<u>Author</u>	<u>Covered country</u>	<u>Type of element</u>	<u>N° of elements</u>	<u>Web reference</u>
<u>Tien Shan landslide inventory</u>	<u>Havenith et al., 2015a</u>	<u>Kazakhstan, Kyrgyz Republic, Tajikistan, Uzbekistan, People’s Republic of China</u>	<u>Polygons</u>	<u>3,462</u>	<u>https://www.sciencedirect.com/science/article/abs/pii/S0169555X15000665?via%3Dihub</u>

<u>Rockslides and Rock Avalanches of Central Asia</u>	<u>Strom and Abdrakhmato v, 2018</u>	<u>Kazakhstan, Kyrgyz Republic, Tajikistan, Uzbekistan, Afghanistan, People's Republic of China</u>	<u>Polygons</u>	<u>986</u>	<u>https://www.sciencedirect.com/book/9780128032046/rockslides-and-rock-avalanches-of-central-asia</u>
<u>Multi-temporal landslide inventory for a study area in Southern Kyrgyz Republic derived from RapidEye satellite time series data (2009 – 2013)</u>	<u>Behling et al., 2014; 2016; 2020</u>	<u>Kyrgyz Republic</u>	<u>Polygons</u>	<u>2,052</u>	<u>https://dataservices.gfz-potsdam.de/panmetaworks/showshort.php?id=escidoc:5085890</u>
<u>The EMCA landslide catalogue Central Asia</u>	<u>Pittore et al., 2018</u>	<u>Kyrgyz Republic, Tajikistan</u>	<u>Points</u>	<u>3,129</u>	<u>https://dataservices.gfz-potsdam.de/panmetaworks/showshort.php?id=escidoc:3657915</u>
<u>Tajikistan landslide database</u>	<u>Institute of Water problems, Hydropower, Engineering and Ecology of Tajikistan (IWPHE)</u>	<u>Tajikistan</u>	<u>Polygons</u>	<u>2,822</u>	<u>N.A.</u>
<u>Uzbekistan landslide inventory</u>	<u>Institute of Seismology of the Academy of Science of Uzbekistan (ISASUZ), State Monitoring Service of the Republic of</u>	<u>Uzbekistan</u>	<u>Polygons/ Points</u>	<u>375</u>	<u>N.A.</u>

	Uzbekistan for hazardous geological processes. Nyazov R.A. 2020, Juliev et al., 2017				
Kazakhstan landslide inventory	Institute of Seismology Limited Liability Partnership (LLP)	Kazakhstan, Kyrgyz Republic	Points	254	N.A.
Global Landslide Catalogue (GLC)	Kirshbaum et al., 2015	Kyrgyz Republic, Tajikistan, Uzbekistan	Points	15	https://svs.gsfc.nasa.gov/4710

282

283 **3.2 Random Forest (RF) model**

284 To generate the landslide susceptibility maps in this work, the Random Forest model (RF) was used. The RF is a
285 nonparametric and multivariate machine learning technique, which was proposed by Breiman (2001), and first
286 used in landslide susceptibility analysis by Brenning (2005). Since then, it has rapidly gained widespread
287 consolidation through many research and case studies, as it is considered a relatively powerful approach in
288 classification, regression, and unsupervised learning (Lagomarsino et al., 2017). Among the advantages of using
289 the RF algorithm, there is the possibility of using numerical and categorical variables at the same time, without
290 assumption on the statistical distribution of their values. Furthermore, RF is acknowledged to be capable of
291 handling implicitly the multicollinearity of variables, identifying the uninfluential (or the detrimental) ones
292 (Breiman, 2001; Brenning, 2005). The RF also automatically performs a validation by building a Receiver
293 Operating Characteristic Curve (ROC Curve) and calculates the relative Area Under the Curve (AUC). AUC is
294 widely used as a quantitative indicator for the predictive effectiveness of susceptibility models: it can range from
295 0.5 (completely random predictions) to 1.0. This model, by means of the bootstrapping technique, also calculates
296 the Out-of-Bag Error (OOBE) for each variable. This parameter measures the relative error that would be
297 committed if a given variable is excluded from the RF classifier. OOBE can be used to assess the relative
298 importance of each independent variable, thus representing a powerful tool to interpret the results and to rank the
299 variables according to their importance (Catani et al., 2013). RF contains a series of binary tree predictors, which
300 are generated by using a random selection of the input data (the independent variables which in LSM studies, are
301 a set of physical parameters representing the predisposing factors), in order to split each binary node (yes/no), and
302 to perform a classification of the target dependent variable (in LSM studies, the presence or absence of landslides).

303 Some of the observations are used for internal testing to evaluate the predictive capability of each predictor tree.
304 This information is used to iterate the procedure hundreds of times by growing other random trees (hence the name
305 “Random Forest”), and to iteratively adjust the prediction effectiveness. Once the best predictor tree is identified,
306 it is applied to the whole study area, to define the LSM. Another important key point of RF is that it has a great
307 predictive performance and runs fast by summarizing many classification trees and this is particularly useful when
308 dealing with large amounts of data.

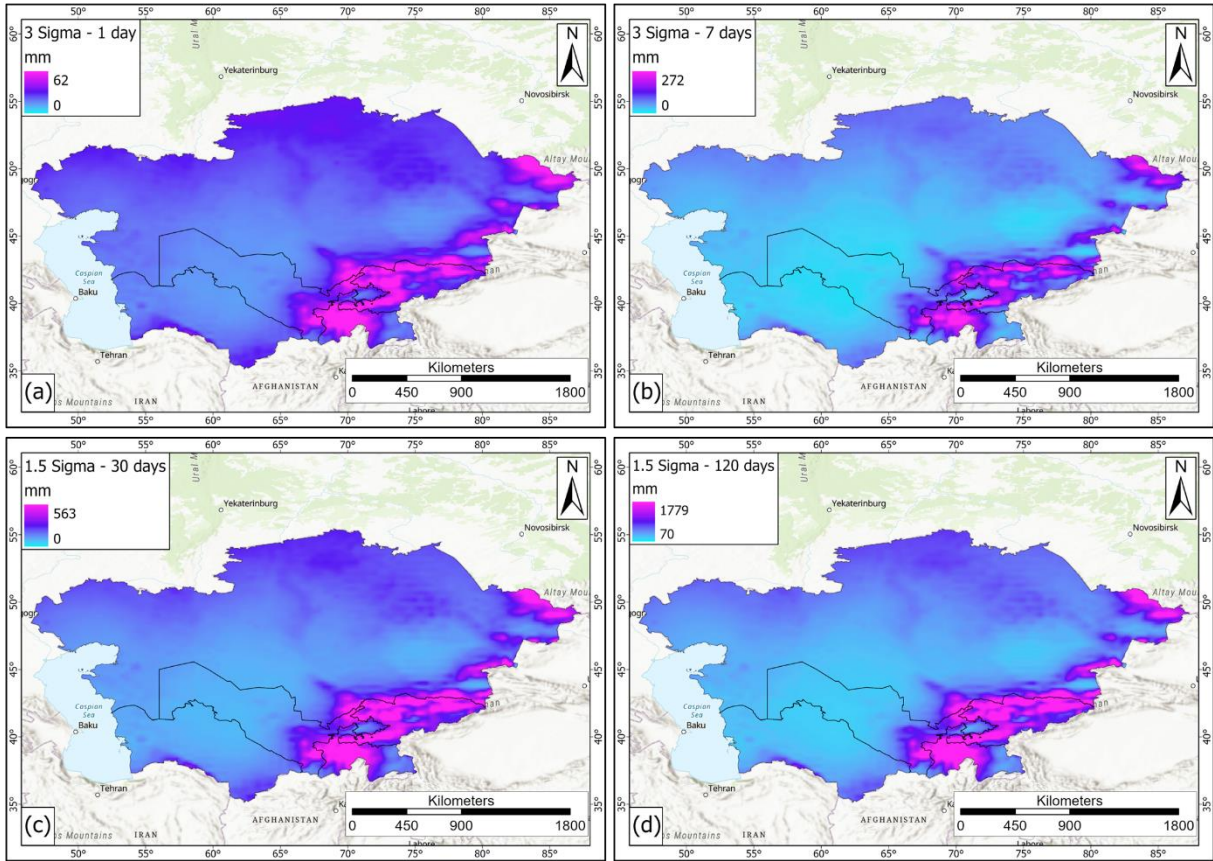
309 **3.3. Selection of independent variables**

310 As independent variables, twenty “basic parameters” were selected in all 5 countries, based on the available data
311 and according to the ones most widely adopted in literature (Catani et al., 2013; Reichenbach et al., 2018). Many
312 of these are DEM-derived products (e.g., elevation, aspect, slope, slope curvature, flow accumulation, Stream
313 Power Index, Topographic Wetness Index, Topographic Position Index). It must be considered that the resolution
314 of the susceptibility maps depends on the resolution of the input data. Therefore, it was decided to use pixels
315 corresponding to the MERIT DEM (Yamazaki et al. 2017) resolution (3” – ca. 90 m at equator and ca 70 m at
316 40° latitude). In addition, the DEM itself was used as a reference map, so that the other parameters were processed
317 to have a perfect overlapping. Therefore, the resulting landslide susceptibility maps will also be perfectly
318 overlapping to it. The variables such as lithology and soil type were rasterized with this resolution by choosing the
319 most frequent value in a reference window. The twenty “basic parameters” used are listed below, including a brief
320 description:

- 321 • MERIT DEM and DEM-derived products: Aspect, Slope Gradient, Total Curvature, Profile Curvature, Planar
322 Curvature, Flow Accumulation, Topographic Wetness Index (TWI), Stream Power Index (SPI), Topographic
323 Position Index (TPI).
- 324 • Lithology, derived from the geological map of the former Soviet Union made by the USGS (Persits et al. 1997).
- 325 • Soil type map from the DSMW database (Copernicus land use; <https://land.copernicus.eu/>).
- 326 • Distance from Faults: it is minimum distance, in meters, between each landslide and the nearest fault. The fault
327 database is derived from the AFEAD catalogue (Styron and Pagani, 2020) and was modified after Poggi et al.,
328 a (in prep.).
- 329 • Distance from Roads: it is minimum distance, in meters, between each landslide and the nearest road. The roads
330 database is derived from Scaini et al., (in prep.).
- 331 • Distance from Rivers: it is minimum distance, in meters, between each landslide and the nearest river. The river
332 network database is derived from Coccia et al., (in prep.).
- 333 • Distance from Hypocentres: it is minimum distance, in meters, between each landslide and the nearest
334 earthquake hypocentre with a magnitude greater than 6.5 (following the methodology adopted by Havenith et
335 al., 2015a). The Hypocentre database was provided by Poggi et al., a (in prep.).
- 336 • Peak Ground Acceleration (PGA): 4 kind of PGA maps according to different return times (475 and 1000 years)
337 and different materials (soil layers and bedrock) to which it refers were created (Poggi et al. b, in prep.).

338 In addition to these “basic parameters”, in this study it was decided to use five parameters related to the propensity
339 of the territory to be affected by precipitation (Fig. 6). These parameters were obtained from the ERA5 database

340 (www.ecmwf.int/en/forecasts/datasets/reanalysis-datasets/era5). [Rainfall distribution maps have been used to](http://www.ecmwf.int/en/forecasts/datasets/reanalysis-datasets/era5)
341 [differentiate the study area based on the rain rate and the distribution of anomalous rainfall events, since more](http://www.ecmwf.int/en/forecasts/datasets/reanalysis-datasets/era5)
342 [rainy areas are more likely to experiment landslide events than those less rainy. At the same time, a rain event with](http://www.ecmwf.int/en/forecasts/datasets/reanalysis-datasets/era5)
343 [a low probability of occurrence can likely trigger a landslide even in less rainy areas, so the probability of some](http://www.ecmwf.int/en/forecasts/datasets/reanalysis-datasets/era5)
344 [extreme rainfall events was calculated as well.](http://www.ecmwf.int/en/forecasts/datasets/reanalysis-datasets/era5)



345 **Figure 6. Rainfall maps from the ERA5 database** (www.ecmwf.int/en/forecasts/datasets/reanalysis-
346 datasets/era5). (a) rainfall amounts corresponding to 3 standard deviations for 1-day rainfall; (b) rainfall amounts
347 corresponding to 3 standard deviations for 7-days rainfall; (c) rainfall amounts corresponding to 1.5 standard
348 deviations for 30-days rainfall; (d) rainfall amounts corresponding to 1.5 standard
349 deviations for 120-days rainfall.
350 Basemap source: Esri, USGS, NOAA.

351 These data span from 1981 to 2020, have a 1-hour temporal resolution (summarized to daily resolution for this
352 work) and a spatial resolution 0.25°. The first parameter is the Mean Annual Precipitation (MAP) map, where, for
353 each pixel, the mean annual precipitation was calculated (Fig. 6). Other maps (named Sigma maps) have been
354 calculated by the spatialization of the approach described in Martelloni et al (2011). In detail, for each rain gauge
355 (represented by the pixels of ERA5 maps in this work) the rain values corresponding to a given standard deviation
356 for several cumulative intervals are defined (e.g., the rain values corresponding to 2 standard deviations of the
357 distribution of 3-days cumulative rainfall):

- 358 • Sigma 1.5 – 120 days: rainfall values corresponding to 1.5 standard deviations of the 120-days cumulative
359 rainfall. They range from 70 mm to 1778.8 mm (Fig. 6a).
- 360 • Sigma 1.5 – 30 days: rainfall values corresponding to 1.5 standard deviations of the 30-days cumulative rainfall.
361 They range from 0 mm to 563.1 mm (Fig. 6b).
- 362 • Sigma 3 – 1 days: rainfall values corresponding to 3 standard deviations of daily cumulative rainfall. They
363 range from 0 mm to 62.2 mm (Fig. 6c).
- 364 • Sigma 3 – 7 days: rainfall values corresponding to 3 standard deviations of the 3-days cumulative rainfall.
365 They range from 0 mm to 271.9 mm (Fig. 6d).

366 The sigma parameters represent the probability of having a given rainfall amount over a defined time interval. In
367 this work, four intervals were selected (1, 7, 30 and 120 days) to consider both short and long rain events, that can
368 lead to the triggering of surficial or deep-seated landslides, respectively. For 1 and 7 days the maps of the rainfall
369 values corresponding to 3 standard deviations over the mean rainfall were selected, to verify if short and very
370 intense rainfall (with a very low probability of occurrence) could influence the slope stability in the study area.
371 Regarding the 30-days and 120-days interval, rainfall values corresponding to 1.5 standard deviation were
372 calculated, in order to assess the influence of longer and less intense rainfalls over slope stability.

373 **3.4. Model optimization**

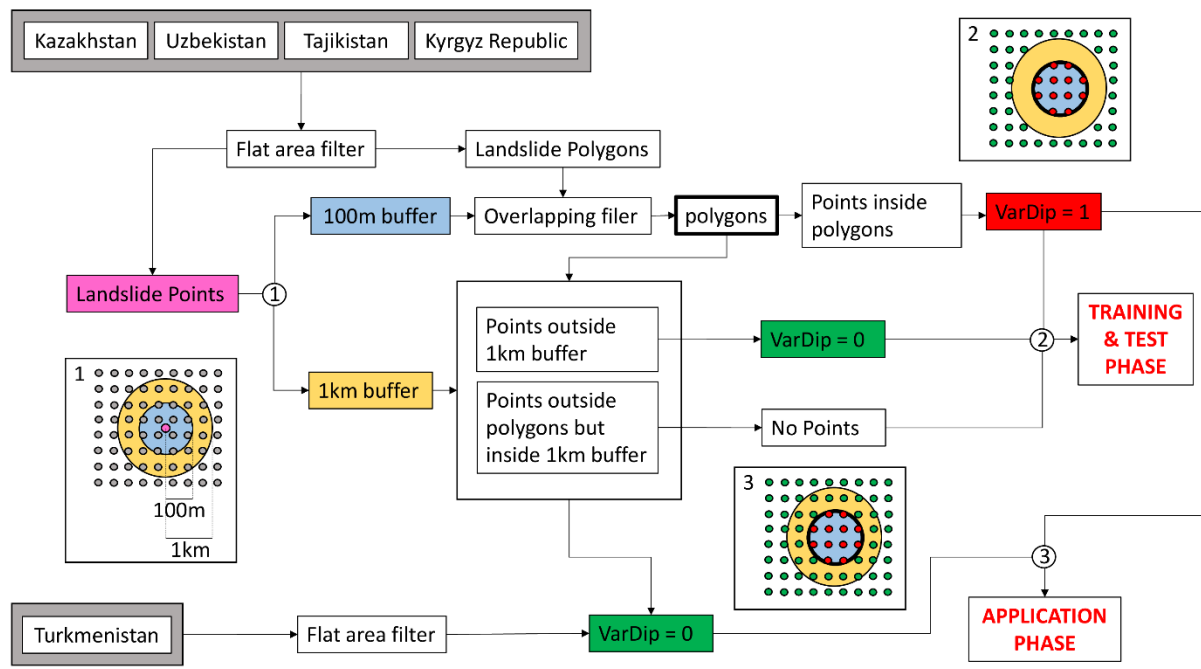
374 3.4.1 Independent variables optimization

375 The LSM was defined using the whole study area, instead of processing each country individually. This choice
376 allowed to overcome the boundary effects associated with the use of independent countries. In addition, a buffer
377 of 10 km was considered around the whole area, to avoid deformation due to boundary effects. These choices were
378 helpful in reducing distortions and improving the quality of the results, but also led to a huge amount of data to be
379 processed. Since the same resolution of the DEM was used for susceptibility assessment, the whole area was
380 divided into about $1.07 * 10^9$ cells and for each cell 26 condition factors and 1 dependent variable were defined;
381 this led to about $2.89 * 10^{10}$ data to be processed. In order to reduce the processing time and avoid computational
382 problems due to the huge amount of data and to the width of the study area, large flat areas were filtered and not
383 considered in the modelling process, since landslides generally take place along slopes (some exceptions to this
384 statement in the area are represented by landslide around the flat Caspian Sea area (Pánek et al., 2016)). For
385 Turkmenistan no landslide database was available, so it was decided to train and test the model only with the other
386 4 countries, to obtain the best predictor model for the available data. The trained model has then been applied to
387 the whole study area, including Turkmenistan, to define the LSM.

388 3.4.2 Landslide Inventory Harmonization

389 Regarding the dependent variables, the landslides inventory was created by merging the data described in section
390 3.1. As a result, this landslide dataset was quite heterogenous, hence an initial control and homogenization phase
391 was necessary. In this framework the landslide data were checked to verify the presence of overlapping polygons
392 or topological errors, which were removed. Since some landslide inventories were composed solely by points,
393 these were mapped only as a “landslide points”, a 100 m buffer was created around them, in order to include them
394 in the model. However, when the points refer to large landslides, which are frequent in the study area, it is possible

395 that part of the body of these landslides is still outside the perimeter achieved with the buffer. To avoid classifying
 396 these areas as non-landslide points, it was decided to create an additional buffer of 1 km around points, used as a
 397 mask where the non-landslide points were not to be selected. This process reduced the probability of pixels
 398 misclassification (e.g., landslide points considered as non-landslide points) during the training of the model. All
 399 the points inside the 1-km buffer were only considered during the model application, as well as point from
 400 Turkmenistan. Some landslide-prone areas were also present in the input inventories; since these were not real
 401 landslides but ‘landslide-prone zones’, these areas were not used to train the susceptibility model but were used in
 402 the validation of the results. This optimization procedure, schematized in Fig. 7, allowed to define an input dataset
 403 of $1.08 \cdot 10^8$ points (along with 27 variables for each point) to be used to define the susceptibility model.

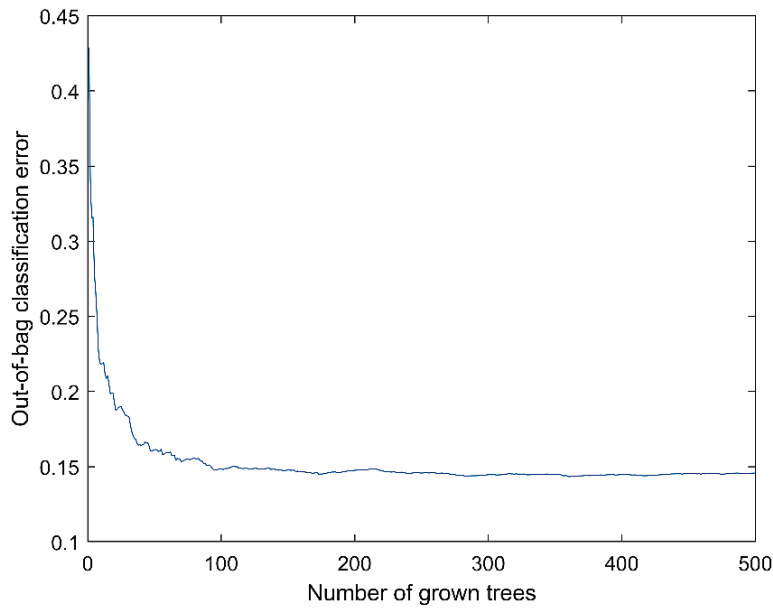


404
 405 **Figure 7. Workflow describing the landslides database harmonization procedure.** In gray: sample points for
 406 RF; pink: landslide points; blue: 100m buffer; yellow: 1km buffer; red: sample points identified as vardip=1; green:
 407 sample points identified as vardip=0; bold black line: landslide body; VarDip=dependent variable.

408 3.4.3 Trees number optimization

409 -A further optimization of the model was performed by the evaluation of the out of bag classification error, i.e.,
 410 the variation of the misclassification probability with the number of grown classification trees.

411 The classification error initially reduces with the increasing of classification trees, then it turns to be stable, so the
 412 definition of the optimal number of classification trees is required to avoid the use of an overgrown forest with an
 413 excessive number of trees (hence with high computational load and time) and without any advantage for the model
 414 (Fig. 78).



415

416 **Figure 78.** Example of out of bag classification error. The error is stable using 100 or more trees.

417 **3.5. Model training**

418 Once all the data were prepared and organized, the algorithm to create the landslide susceptibility maps was
 419 developed. A crucial step in LSM analysis is the approach used to sample the variables to train and validate the
 420 model. As in any other statistical procedures, the size of the dataset influences the results, therefore the higher the
 421 number of samples to perform the statistical calibration/validation of the model, the more reliable are the obtained
 422 results. To avoid a generalized hazard overestimation, Catani et al. (2013) demonstrated that a random sampling
 423 improves the predictive capability of the map, and that the susceptibility model should also be trained/validated
 424 with respect to information about non-landslide locations. Regarding the proportion between the calibration and
 425 validation dataset samples, it is common practice to split them according to a 70/30 ratio. Therefore, using ESRI
 426 ArcGIS Pro software, all the variables were sampled pixel by pixel, after which, with the Matlab software, from
 427 the total of the sampled points, all the points within a landslide and a same amount of randomly chosen non-
 428 landslide points were extracted. This input dataset was divided into two parts, 70% of the data (calibration dataset)
 429 was used for the training phase, and the remaining 30% (validation dataset) for the testing phase. The selection
 430 and division were randomly repeated 5 times, in order to assess the stability of the model to the variation of the
 431 training and testing datasets, hence, to verify the absence of overfitting issues. Each one of these datasets was
 432 created to be equally composed by pixel within a known landslide and pixel outside a landslide. All these data
 433 were then used to train and test the algorithm created to predict the landslide susceptibility of the whole area. The
 434 best predictor model identified in the training phases was then applied to all the available data (also for
 435 Turkmenistan and for the 1-km buffer area around the point-object landslides) for the development of the
 436 susceptibility map on the whole Central Asia area. The results obtained from the application of the aforementioned
 437 methodology are the susceptibility map, the ROC (Receiver Operating Characteristic) curves with their AUC (Area
 438 Under the Curve) values, and the histogram of the importance of variables. ROC and AUC are used to verify the
 439 quality of the landslide susceptibility model, both by graphical and analytical approach. Due to the high volume

440 of data, their variety, values, and heterogeneity a specific algorithm was created for this work, that was set to be
441 able to perform several activities:

- 442 • Reading and properly formatting the input data and then dividing them between independent and
443 dependent variables.
- 444 • Automatically and randomly selecting locations associated with landslides or outside landslides to create
445 the training and test datasets.
- 446 • Identifying the best predictor and evaluating its performances by the calculation of the misclassification
447 probability of the values calculated by the model.
- 448 • Evaluating the overall performances of the model by the mean of ROC and AUC.
- 449 • Identifying the importance of the parameters in landslide susceptibility.
- 450 • Applying the model to the whole study area, calculate the probability of classification (landslide or non-
451 landslide) of each pixel and extraction of the final map in raster format.

452 The algorithm was set to work in classification mode, e.g., for each pixel a value (1 or 0) is assigned to identify
453 the presence or absence of a landslides (dependent variable), along with the values of the independent variables.
454 Using these data, the RF model identifies the best association of independent variables linked to presence or
455 absence of landslides (landslide susceptibility prediction model). The prediction model is then applied to all the
456 pixels of the investigated area, and the probability of each pixel to be classified as landslide (or non-landslide)
457 pixel is evaluated. These probability values are those used to create the landslide susceptibility maps. It must be
458 noticed that the landslide inventories adopted to train the RF rarely reported the type of landslide, so the LSMs
459 must be considered not related to a specific type of landslide.

460 **3.6. Model validation**

461 To verify the quality of the susceptibility models, beside the AUC value previously reported, a confusion matrix
462 for the four countries where the model was trained was created (Fig. 89). In each matrix the predicted landslide
463 classes are compared with the ground truth to verify the presence of significant misclassification error. In all the
464 matrix the value 1 represent the presence of landslide, the value 0 represents the absence of landslides; the numbers
465 in each cell represent the number of pixels classified in that combination of 0 and 1, according to this scheme (the
466 first number represent the predicted class, the second number the ground truth):

- 467 • 0-0 (True negative): pixels outside any landslides are correctly identified as no-landslide pixels by the
468 model.
- 469 • 1-1 (True positive): pixels inside a landslide are correctly identified as landslide pixels by the model.
- 470 • 0-1 (False negative): pixels inside a landslide are wrongly identified as no-landslide pixels by the model.
- 471 • 1-0 (False positive): pixels outside any landslides are wrongly identified as landslide pixels by the model.

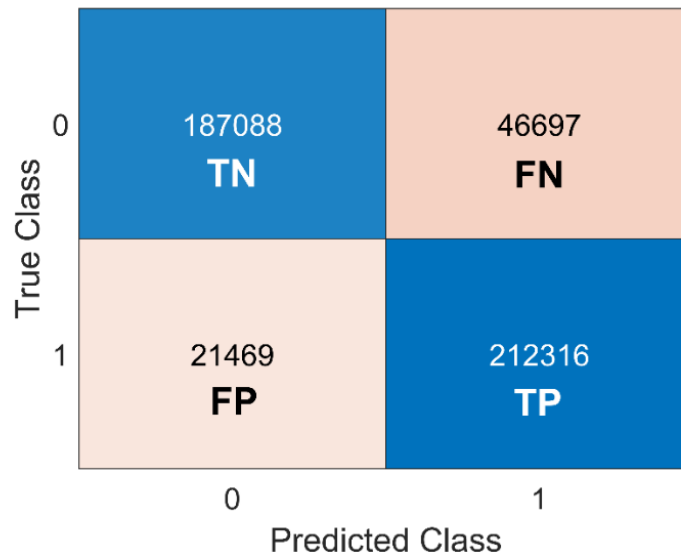


Figure 89. Confusion matrix for the four countries where the model was trained.

The 0-0 and 1-1 combinations represent well classified pixels (blue cells in Fig. 8), while 0-1 and 1-0 represent misclassification error (light red cells in Fig. 8). Since this matrix needs some ground-truth parameters (True classes), it can be applied only where the presence or absence of landslides is known. For this reason, in this work, this matrix was calculated considering only the test dataset. A further control of the results was made using the areas prone to landslides identified in the used landslide inventories.

3.7. Landslide susceptibility and elements at risk

The susceptibility map of the study area was intersected with the elements at risk, consisting of roads railways, population, to analyse the landslide susceptibility distribution in the area covered by elements at risk. The database of element at risk was provided by Scaini et al., in prep. In order to perform the analysis several approaches were defined based on the different types of elements at risk. the population and buildings data were based on a grid with a spatial resolution of 1km², defining for each cell the number of inhabitants, the number of different types of buildings (residential, commercial, industrial, education and healthcare), and the mean susceptibility class by means of spatial statistics between input databases (population buildings data and susceptibility map). The results carried out from the spatial statistics allowed to assess the people and buildings distribution within each susceptibility class. On the contrary, the linear elements (roads and railways) were divided in segments with 1 km in length, and buffered, setting a distance parameter equal to 100 m. After this preliminary process, the spatial statistics with the landslide susceptibility have been carried out.

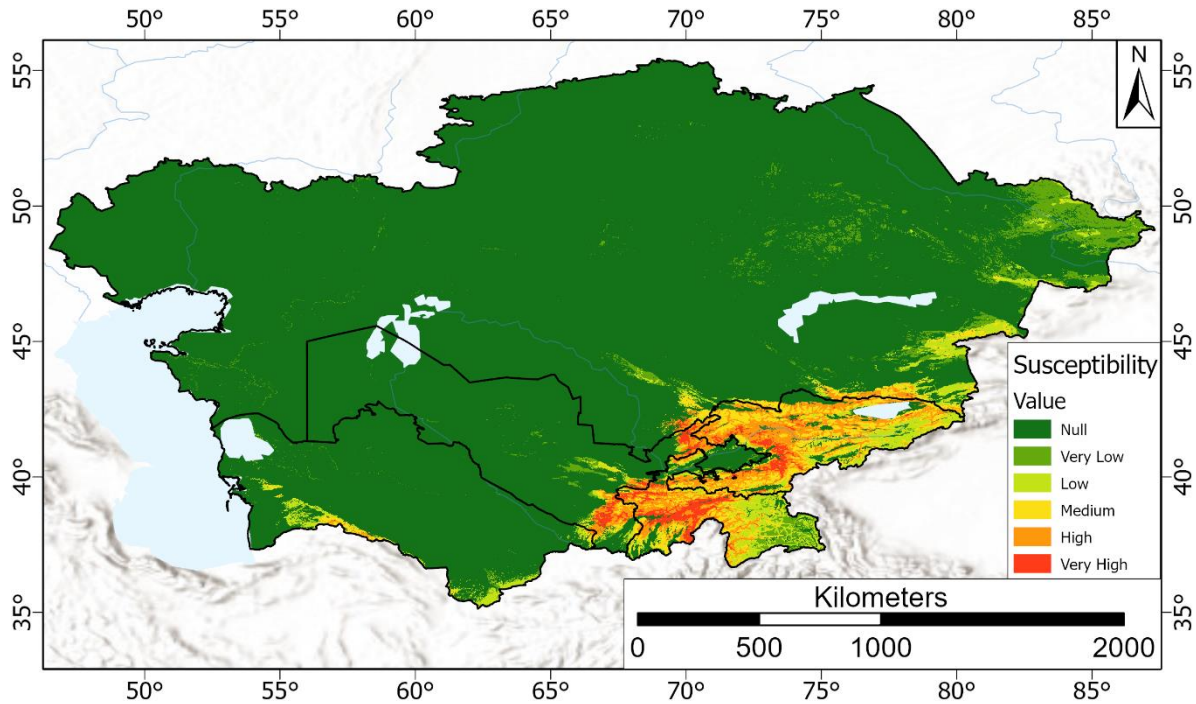
4. Results

4.1 Susceptibility map

501 In the map presented in the following Figures 9-10 and 10-11, the susceptibility values, ranging from 0 to 1, were
502 classified into five classes (Table 2-Table). Here the corresponding extension and percentage of the study area are
503 also reported, showing that the most frequent susceptibility class for the whole study area is the null class (=87.8%;
504 landslides generally don't occur in flat areas), followed by low and medium classes. Only the 4% of the central
505 Asian territory is represented by areas with high and very high landslide susceptibility (Table 2-Table).

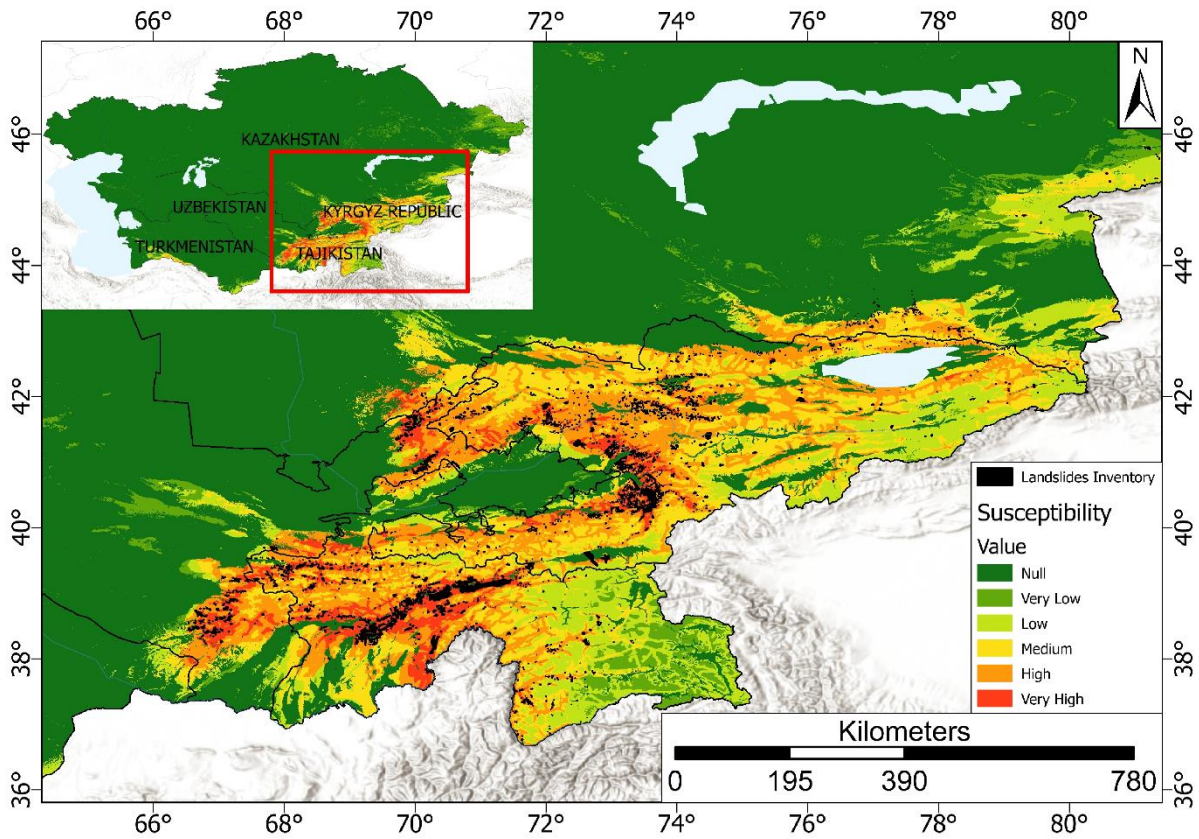
ha forma

ha forma



506

507 **Figure 9-10.** Landslide susceptibility map of Central Asia. Basemap source: Esri, USGS, NOAA.



508

509 **Figure 10.** Detail of the landslide susceptibility map with the overlapping landslide polygons (in black).
 510 On the top left the detailed area with respect to the central Asian territory. Basemap source: Esri, USGS, NOAA.

511 **Table 23.** Landslide susceptibility class intervals, corresponding area, and percentage with respect to CA.

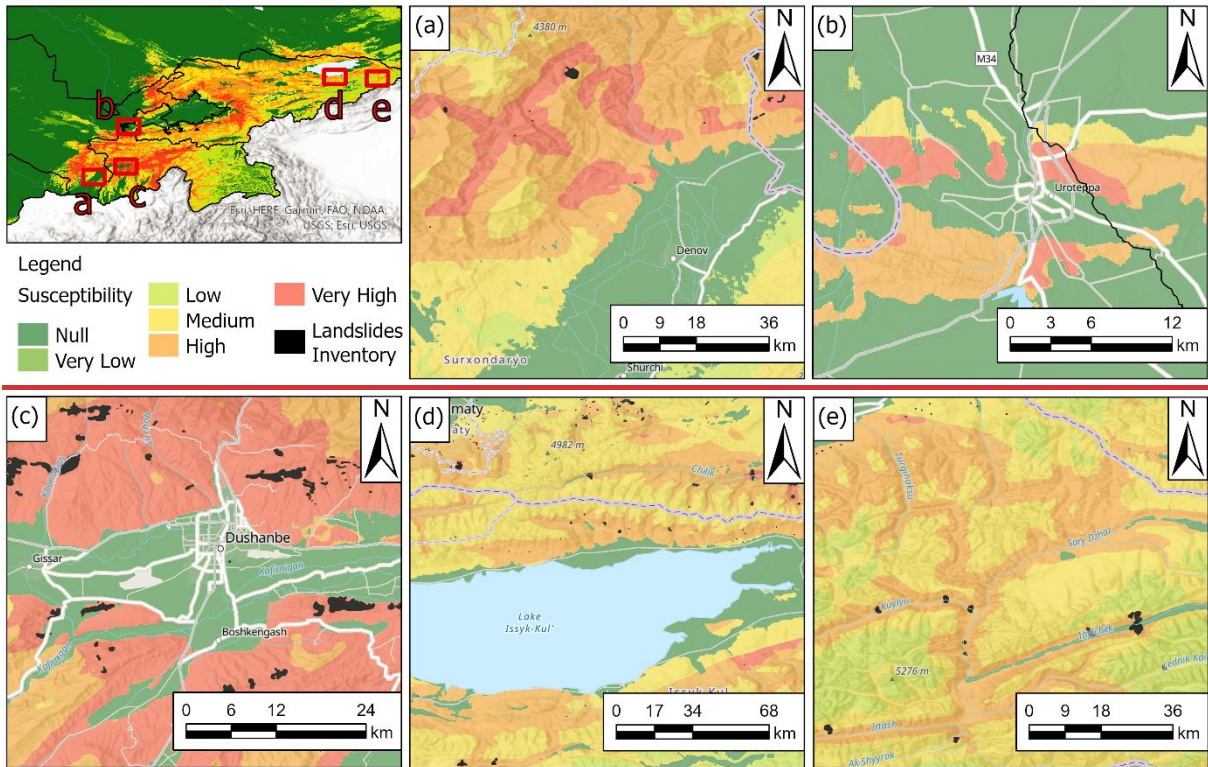
Susceptibility class	Landslide spatial probability interval	Corresponding area (km ²)	Corresponding percentage of CA (%)
Null	0 - 0.05	2,889,481.2	87.8
Very Low	0.05 - 0.25	94,674.7	2.9
Low	0.25 - 0.35	85,294.1	2.6
Medium	0.35 - 0.45	87,528.5	2.7
High	0.45 - 0.6	99,689.8	3
Very High	0.6 - 1	31,436.4	1

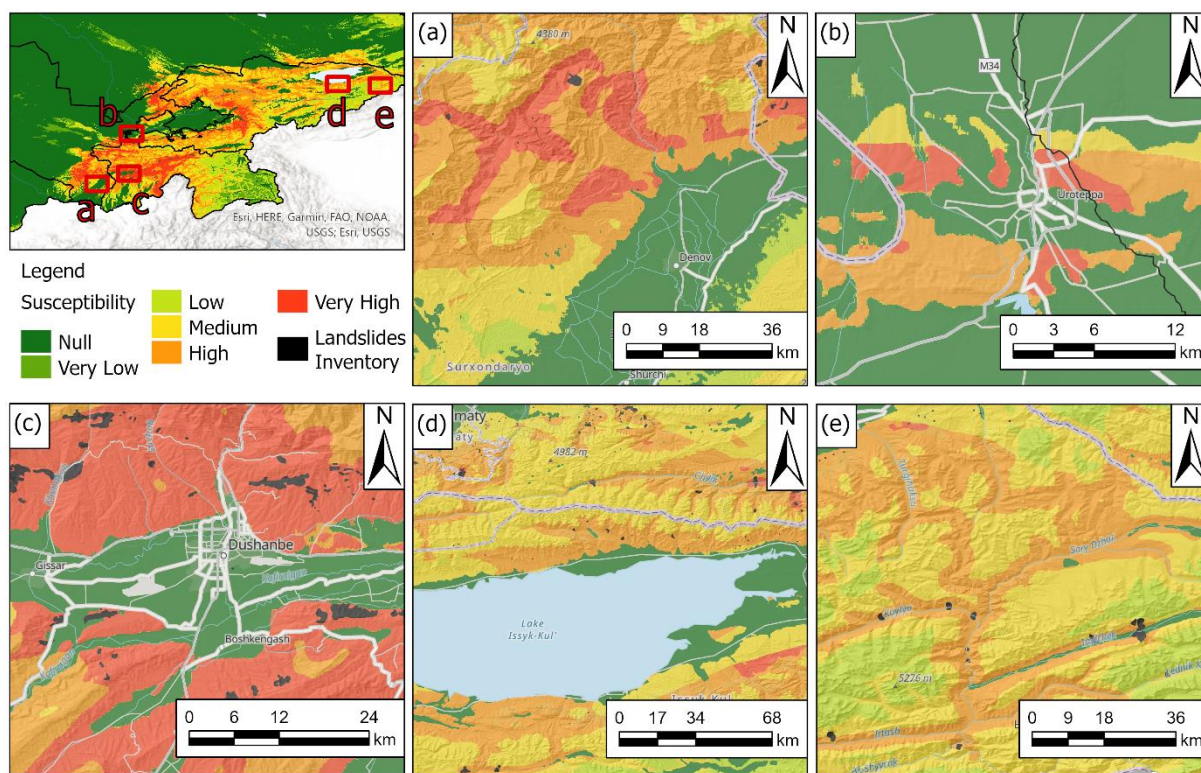
512

513 In Fig. 11, the susceptibility maps of five selected areas are displayed [to better show the details result of the](#)
 514 [susceptibility assessment, and its comparison with mapped -landslides in different geomorphological contexts of](#)
 515 [the study area](#). From these details it is possible to ascertain the high usefulness of the landslide susceptibility map
 516 realized by applying the Random Forest model, which, mainly based on the hydro-geomorphological properties,
 517 can establish the degree of susceptibility even in areas where there is no awareness of the predisposition to
 518 instability due to the absence of reported landslides.

519 In particular:

- 520 • Fig. 4a-12a shows the area north of the city of Denau, in the south-east of Uzbekistan, which is characterized
521 by a high susceptibility, despite the almost total absence of mapped landslides.
- 522 • Fig. 4b-12b shows a detail of the city of Ura-Tube, in the North-West of Tajikistan, where there are not any
523 known landslides, but a high susceptibility has been obtained in the surrounding mountain relief.
- 524 • In Fig. 4c-12c there is a close-up on the city of Dushanbe, the capital of Tajikistan, where close to roads
525 and inhabited centres a high landslides susceptibility is observed.
- 526 • The shores of Lake Issyk-Kul in the Kyrgyz Republic, shown in Fig. 4d-12d, are generally flat areas, with a
527 low or null landslide susceptibility but in the central zone.
- 528 • Finally, Fig. 4e-12e shows a detail of the western area of the Kyrgyz Republic, where a high landslide
529 susceptibility is observed along the slopes adjacent to the river network.



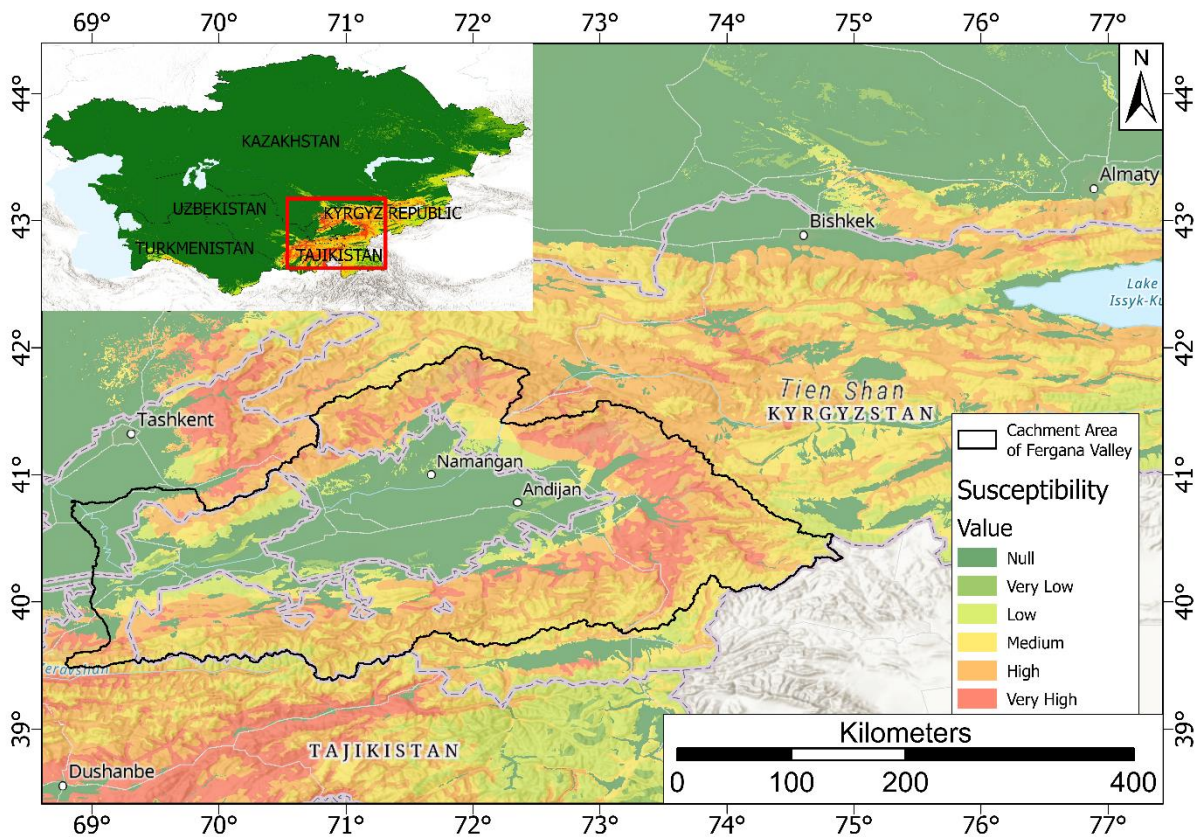


531
 532 **Figure 14.12.** Details of the landslide susceptibility map. (a) the city of Denau, Uzbekistan; (b) the city of Ura-
 533 Tube, Tajikistan; (c) the city of Dushanbe, Kyrgyz Republic; (d) the Lake Issyk-Kul, Kyrgyz Republic; (e) the
 534 eastern area of the Kyrgyz Republic. Black polygons represent landslide areas from the adopted landslide
 535 inventories. Basemap source: Esri, USGS, NOAA.

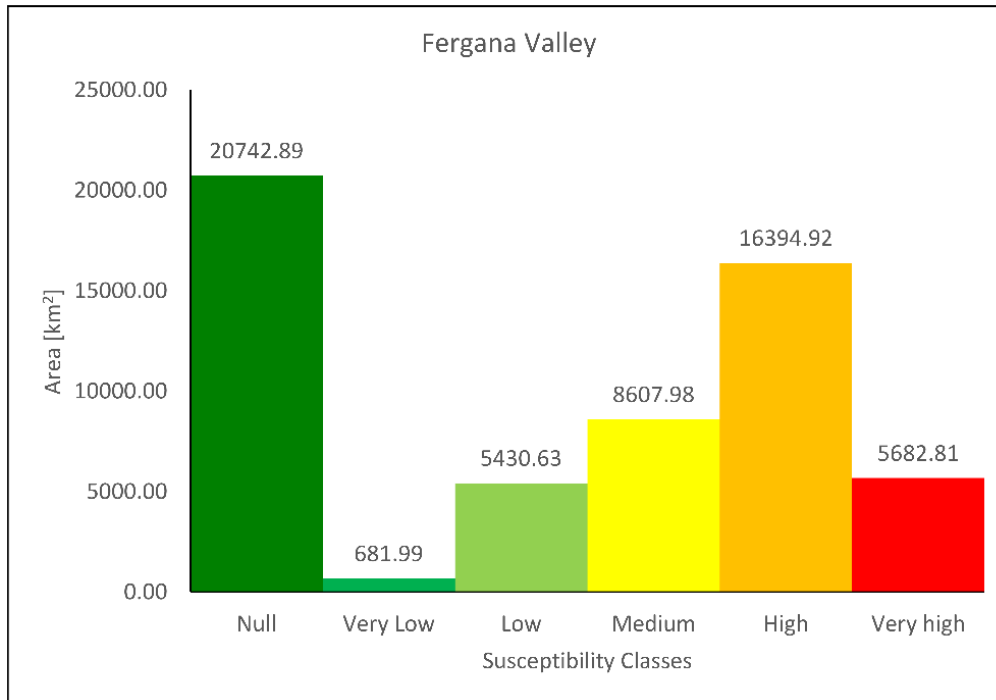
536 **4.2 The Fergana valley mountainous rim**

537 The Fergana valley spreads across eastern Uzbekistan, southern Kyrgyz Republic, and northern Tajikistan (Fig.
 538 14.13). It is one of the largest intermountain depressions in Central Asia, located between the mountain systems of
 539 the Chatkal-Kuraminsk ranges in the north and the Turkestan--Alai in the south. The two main rivers, the Naryn
 540 and the Kara Darya, flow into the valley and unite forming the Syr Darya. In this area landslides represent one of
 541 the major natural hazards due to their frequent (seasonal) occurrence across large areas: in fact, they are particularly
 542 concentrated in a range of altitudes between 700 and 2000 m along the topographically rising rim below its
 543 transition into higher mountainous terrain (Roessner et al., 2000; 2004; 2005; Behling et al., 2014; 2016). This
 544 region is quite densely populated, and landslides lead almost every year to damage of settlements and infrastructure
 545 and loss of human life (Schloegel et al., 2011; Piroton et al. 2020). In this area landslide activity is caused by
 546 complex interactions between tectonic, geological, geomorphological and hydrometeorological factors (Havenith
 547 et al., 2015a, b). In the Fergana valley rim mass movements are often characterized by deep and steep scarps,
 548 mobilize weakly consolidated sediments of Tertiary or Quaternary age, including loess deposits (Piroton et al.,
 549 2020). These kinds of landslides are particularly deadly, and can be triggered by a combination of long-term slope
 550 destabilization factors (e.g., rainfall and snowmelt) and short-term triggers (Danneels et al., 2008). Slope landslide
 551 susceptibility was analysed in this area using the previously mentioned methodologies. Fig. 14.13 shows the
 552 particular about the landslide susceptibility map obtained for the Fergana Valley, while Fig. 14.14 reports the

553 histogram of the area occupied by each susceptibility class. It can be observed that the most frequent susceptibility
 554 class in the Fergana Valley area is the Null class, which covers an area of about 20,743 km², that is 36% of the
 555 valley. The Very Low and Low classes occupy respectively an area of 681 km² (1.2%) and 5,431 km² (9.4%). The
 556 Medium class instead extends for about 8,608 km², namely the 15% of the total. The High class instead extends
 557 for about 16,395 km², that is 28.5% of the total and finally, the remaining 9.9% of the national territory, that is
 558 about 5,683 km², is classified in the Very High class.



559
 560 **Figure 1213.** Detail of the landslide susceptibility map obtained for the Fergana Valley. Basemap source:
 561 Esri, USGS, NOAA.

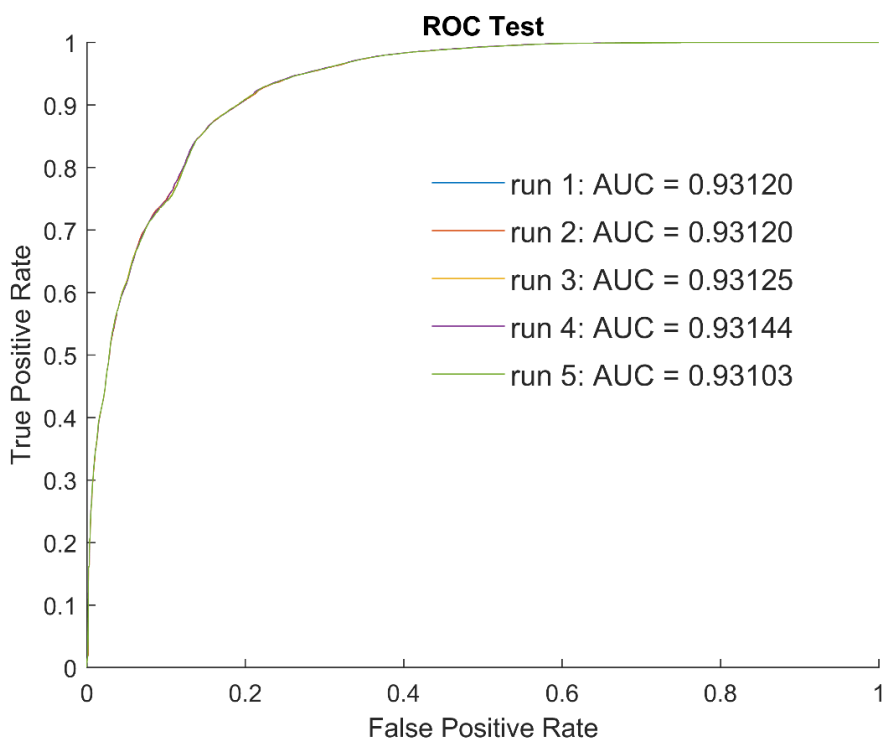


562

563 **Figure 1314.** Frequency histogram of susceptibility classes obtained for the Fergana Valley mountainous
 564 **rim.** On each bar the corresponding area in km² is reported.

565 **4.3 Trained model performances and conditioning factors relevance**

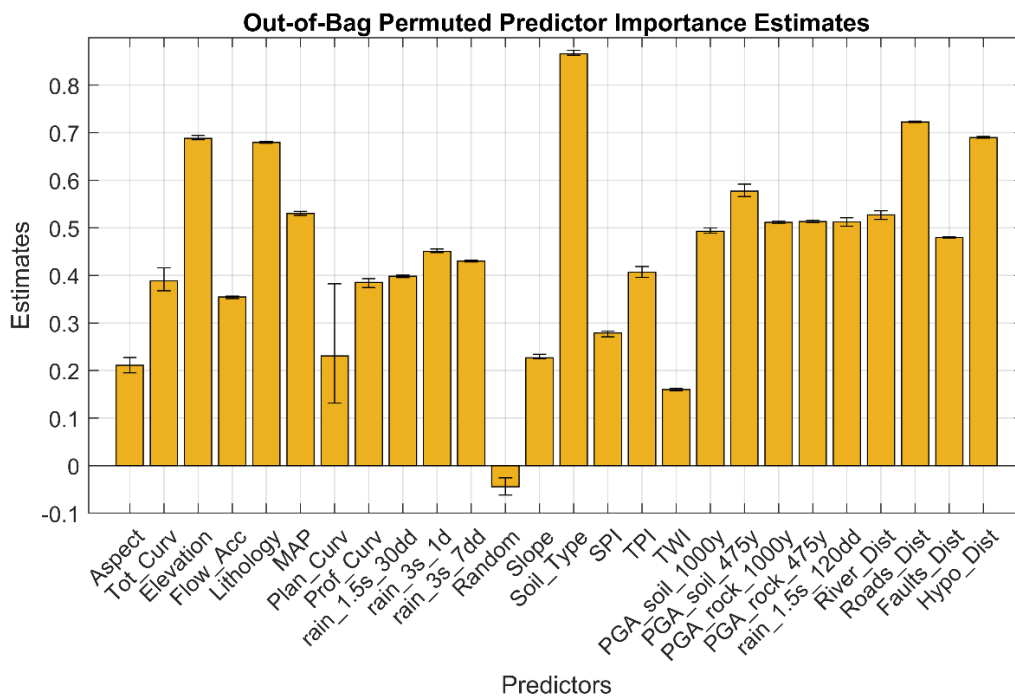
566 The RF was initially trained setting 1,000 trees to be growth. After the first run, the analysis of the out-of-bag error
 567 revealed that misclassification probability reduced significantly with a forest of 150 trees and then reduced slightly
 568 up to 500 trees, then it turned to be stable, so the optimal number of trees was set equal to 500 and used for all the
 569 simulations. As described above, the model was run 5 times to verify its stability and the AUC values ranged from
 570 0.93103 to 0.93144 (Fig. 1415), with a mean value of 0.93122 and a standard deviation of 0.00015. The low
 571 variance of the AUC values confirmed the stability of the model and its applicability to the whole area. As we can
 572 see in the ranking of the susceptibility parameters, reported in Fig. 1516, soil type, lithology, elevation, the distance
 573 from roads and hypocentres plays a crucial role in landslide susceptibility, since they are the five most influencing
 574 factors (for the four countries where the model was trained). Rainfall parameters are also important in the obtained
 575 landslide susceptibility, in particularly the 1-day rainfall value that shows the highest importance among the
 576 rainfall parameters. Also, the PGA maps are a relevant factor, while TWI and slope curvature are the less important
 577 parameters. The average AUC value of the models is 0.93122, indicating their very good quality. Such high AUC
 578 values can indicate the presence of overfitting issues, but this hypothesis can be discarded, since the random
 579 variable resulted without any importance in landslide susceptibility (negative OOB value).



580

581

Figure 1415. ROC curve and relative AUC value for each model run (test samples).



582

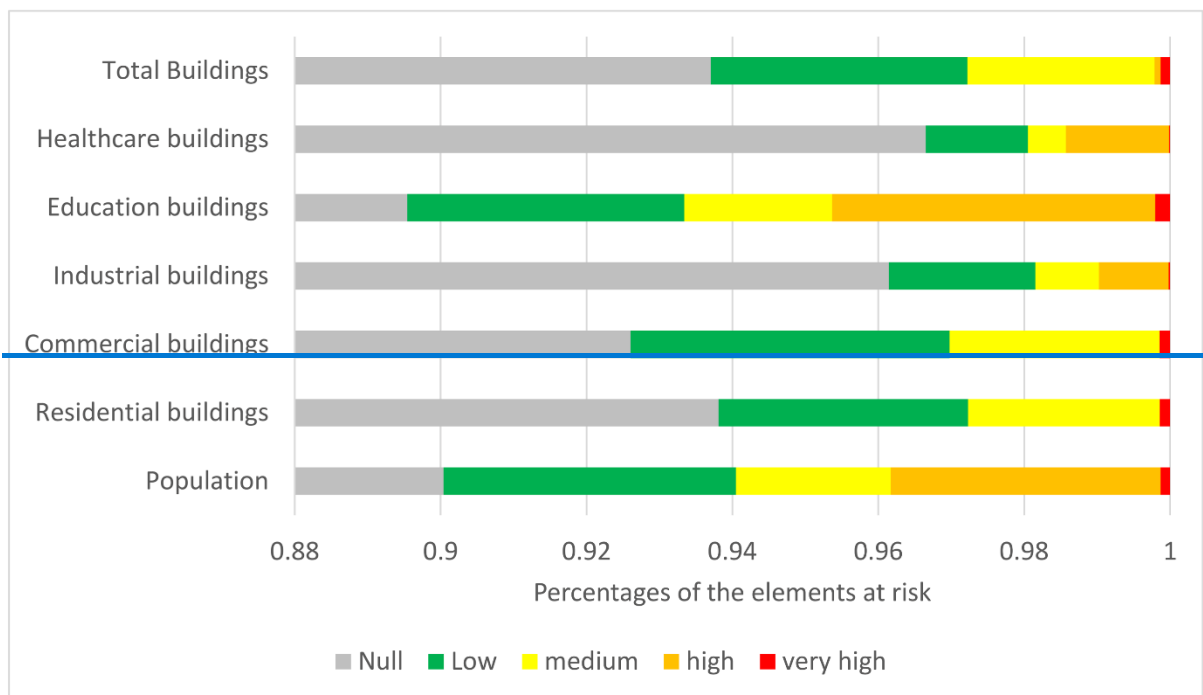
Figure 1516. Variable importance in landslide susceptibility for the four countries where the model was trained. From the 5 model runs, the results were averaged and displayed in this image, with the error bars showing the maximum and the minimum value obtained.

586 **4.4 Landslide susceptibility and exposed elements**

587 Concerning the outcomes regarding buildings and population, they are represented by Table 3, in which for each
 588 susceptibility class the number of people and the number of different building types are reported, and in the bar
 589 diagram of (Fig. 16). The obtained results about roads and railways are reported in Table 4 and in Fig. 17.

590 **Table 3. Population and buildings distribution in each landslide susceptibility class.**

Element at risk	Landslide susceptibility				
	Null	Low	medium	high	very high
Population	68,422,152	3,046,892	1,612,487	2,812,081	97,934
Residential buildings	8,769,270	319,776	245,754	386,628	12,753
Commercial buildings	2,196,037	103,745	68,187	68,232	3,410
Industrial buildings	705,352	14,776	6396	7024	110
Education buildings	42,472	1802	960	2102	96
Healthcare buildings	15,476	224	84	226	2



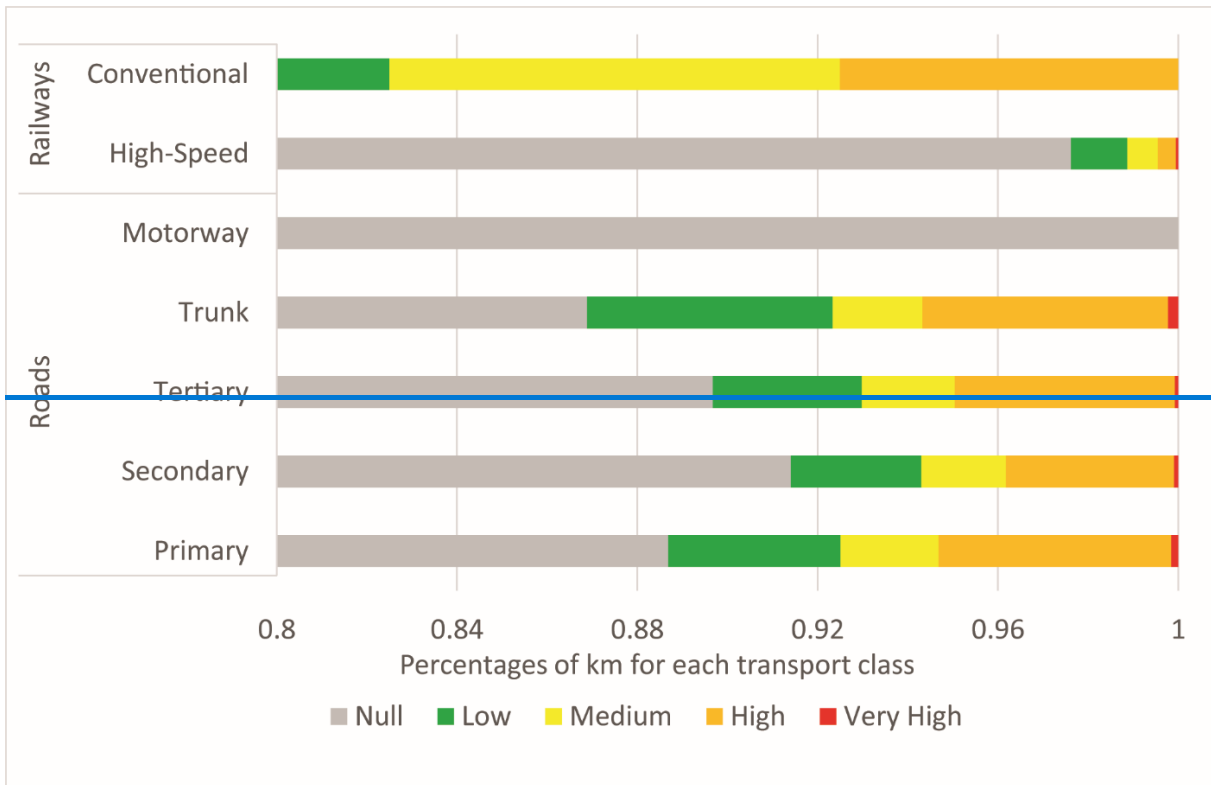
594 **Figure 16. Percentage of the Element at risk falling within landslide susceptibility classified areas.**

598

Table 4. Distribution (corresponding km) of road and railway classes in landslide susceptibility classes.

		Null	Low	Medium	High	Very High
Road Class	Primary	15,000	646	368	873	26
	Secondary	28,773	911	589	1,173	30
	Tertiary	71,515	2,637	1,643	3,898	55
	Trunk	30,058	1,887	686	1,887	77
	Motorway	1,732	+	+	+	+
Railway Class	High Speed	45,866	589	317	187	25
	Conventional	128	4	16	12	+

599



600

601

Figure 17. Landslide susceptibility distribution for each transportation class.

602

5. Discussion

603

Landslide susceptibility

604

The main issue affecting the used random forest model is the need of an adequate training dataset to properly

605

calibrate the predictor model. The first step of the work has been the homogenization of the landslide data, the

606

used landslide inventory was created starting from different sources, hence, with quite non-homogeneous (e.g., in

607

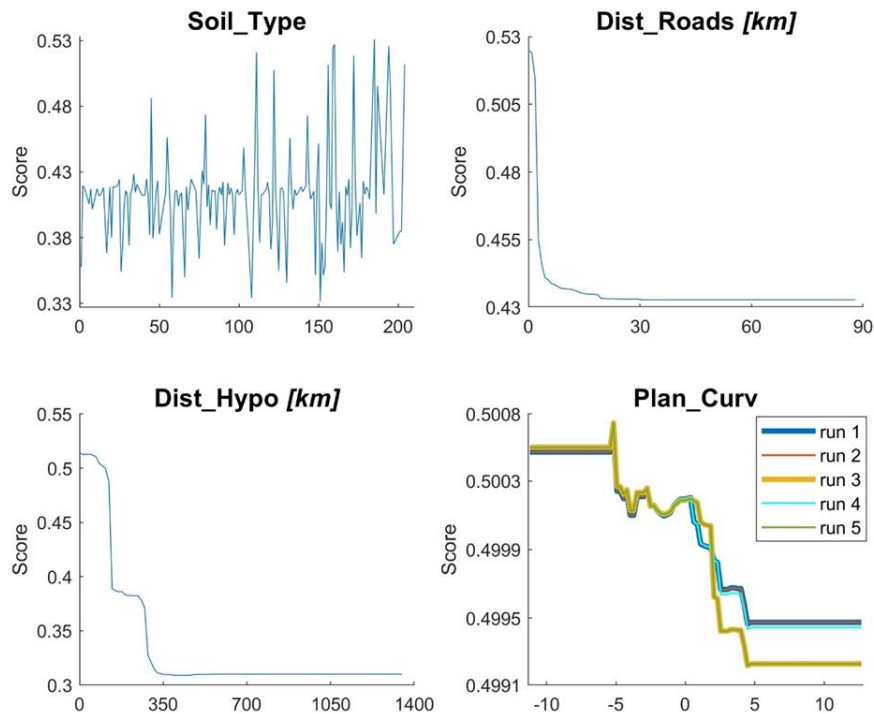
some cases the whole landslide perimeter was available, in other cases only a point representing the source area

608 of each landslide was provided, without info about the landslide dimension or propagation distance; more in
609 general there were few or no data about the landslide type or triggering causes). The lack of some data about the
610 landslides, or the partial or complete lack of landslides as in Kazakhstan and Turkmenistan, could lead to
611 underestimate the real landslide hazard of the studied countries, since some points could have been wrongly
612 classified (e.g., they have been considered as no landslide areas, but it was possible that a not reported landslide
613 was present). Furthermore, not all the adopted landslide inventories included information regarding the landslide
614 types, leading to the creation of a general landslide susceptibility map, where all the types of landslides are
615 considered. The created maps have been validated only using the available landslide dataset, providing good results
616 and highlighting the good prediction capability of the model. Anyway, an in-situ validation in some sample areas
617 can help to verify the quality of the results. As previously stated, for Turkmenistan there was no landslide inventory
618 available to train the RF model, therefore the corresponding LSM was obtained applying the model trained for the
619 other four countries. The lack of landslide data did not allow any validation of the result or estimation of the quality
620 of the susceptibility map of Turkmenistan. Furthermore, applying the model developed for the other countries, the
621 same importance of the conditioning factors (e.g., the independent variables) was assumed. For these reasons, the
622 landslide susceptibility map for Turkmenistan is more uncertain than those evaluated for the other four countries.
623 Among the used conditioning factors, soil type, distance from roads and distance from hypocentres resulted to be
624 the most influencing factors in slope stability, while planar curvature resulted with a high variability of its
625 importance. These parameters have been hence more deeply analysed to understand how they influence landslide
626 susceptibility. According to the partial dependency plots (Fig. 1817), which show how the values of each
627 conditioning factor influence the landslide susceptibility, the soil types more related to landslides are lithosols and
628 cambisols, low thickness soils limited in depth by a continuous coherent and hard rock layer, located in steeply
629 slopes, with more than 30% of slope gradient. While the classes that have the lowest importance score are fluvisols
630 (young soils in alluvial deposits), xerosols (mainly arid clay) and chernozems (soils rich in organic matter), each
631 situated in flat to hilly areas, with less than 30% of slope gradient. Distance from roads, as expected, is important
632 for low values since the importance score is maximum for distance close to zero and it decrease exponentially with
633 the increasing of the distance. A similar behaviour can be noted with the distance from hypocentres, meaning that
634 areas close to hypocentres (within a radius of about 25 km) can more easily experience landslide phenomena in
635 case of future earthquakes. The partial dependency plot of planar curvature showed that the variability highlighted
636 in Fig. 16, is in fact, not so relevant since the range of the importance score is quite limited (values ranging from
637 0.4992 to 0.5008). In addition, it is possible noticing that negative values of planar curvature have a higher
638 importance score than zero values or positive values, meaning that concave slopes are more prone to landslide
639 than plain or convex surfaces.

640 *Landslide susceptibility and exposed elements*

641 ~~The integration of susceptibility map with the maps of element at risk and communication router allowed to~~
642 ~~identify those elements potentially more prone to landslide hazard, even of with some limitations. The obtained~~
643 ~~results are indeed influenced by the input data (the susceptibility maps and the elements at risk databases).~~

644 ~~The buffering procedures on roads and railways could overestimated or underestimated the susceptibility~~
645 ~~distribution in some cases, likewise the analysis at 1km² resolution on population and buildings could led to an~~
646 ~~exaggeration in the assessment of elements distribution in each class of landslide susceptibility.~~



647

648 **Figure 1817. Partial dependence plots.**

649 ~~Nevertheless, the adopted approaches represented the only way to obtain an analysis as much accurate as possible~~
650 ~~respect to the input databases. In this perspective, the detail of analyses could be improve focusing both on the~~
651 ~~refinement of the analysis resolution (e.g., population and buildings) and on the elements at risk that are not located~~
652 ~~in flat areas, where the landslide susceptibility is surely 0 or NULL.~~

653 **6. Conclusions**

654 ~~In this work a new landslide susceptibility assessment of Central Asia was carried out. With respect to previous~~
655 ~~works, in this research a unique map was created and with a higher resolution, in order to avoid boundary effects,~~
656 ~~to get to more homogeneous and with better resolution results. The used approach allowed also to identify the~~
657 ~~most relevant landslides predisposing factors: soil type distance from roads and hypocentres. The size and the~~
658 ~~heterogeneity of the study area required the use of many input variables, some of them never used before in~~
659 ~~landslide hazard assessment, and the elaboration of a high volume of data, as well as the adoption of some specific~~
660 ~~procedure to accounting for the presence of heterogeneities and uncertainties in the input data, as the presence of~~
661 ~~point landslides. The comparison with elements at risk and communication routes allowed a better assessment of~~
662 ~~landslide hazard in the area, which can be useful to improve the land use management and to reduce the risk. The~~
663 ~~main limitation of the work is related to absence of data about type and geometry for several landslides; in the~~
664 ~~future a better input landslide inventory could help get to different susceptibility maps for different landslide types.~~

665 ~~Another limitation is due to the absence of any information about the presence or absence of landslides in~~
666 ~~Turkmenistan, which did not allow any clear validation of the results for this country.~~

667 In this work a new landslide susceptibility assessment of Central Asia was carried out as a part of a multi-hazard
668 approach in the framework of the SFRARR Project (“Strengthening Financial Resilience and Accelerating Risk
669 Reduction in Central Asia”). Over 13,000 landslide elements were implemented in a Random Forest model to
670 create a unique map in order to avoid boundary effects and obtain, a more homogeneous and with higher resolution
671 susceptibility map with respect to previous works. The used approach allowed also to identify the most relevant
672 landslides predisposing factors: soil type, distance from roads and hypocentres. The size and the heterogeneity of
673 the study area required the use of many input variables (some of them never used before in landslide susceptibility
674 assessment), and the elaboration of a high volume of data, as well as the adoption of specific procedures to account
675 for the presence of heterogeneities and uncertainties in the input data (such as the presence of polygon and point
676 landslides). The main limitation of the work is related to absence of data about type and geometry for several
677 landslides; in the future a better input landslide inventory could help get to different susceptibility maps for
678 different landslide types. Another limitation is due to the absence of any information about the presence or absence
679 of landslides in Turkmenistan, which did not allow any clear validation of the results for this country. The results
680 provide a useful tool for landslide scientists, practitioners, and administrators involved in land use-planning
681 activities and risk reduction strategies in Central Asia.

682 **Code and data availability.** The landslide susceptibility model was implemented by using the cited landslide
683 inventory maps, published by the following authors: Behling et al., 2014, 2016, 2020; Havenith et al., 2015a;
684 Kirshbaum et al., 2015; Pittore et al., 2018; Strom and Abdrakhmatov, 2018. Other data implemented in the model,
685 such as MERIT DEM, geological formations, Active Fault Database, soil type map, rainfall maps are available
686 from Yamazaki et al. 2017, Persits et al., 1997, Styron and Pagani, 2020, <https://land.copernicus.eu/>,
687 www.ecmwf.int/en/forecasts/datasets/reanalysis-datasets/era5, respectively. The database on infrastructures, river
688 network, PGA and other landslide inventories were provided by the SFRAAR project partners: RED (Risk,
689 Engineering + Development – Pavia, Italy), OGS (National Institute of Oceanography and Experimental
690 Geophysics, Seismological Research Center, Trieste, Italy), IWPHE (Institute of Water problems, Hydropower,
691 Engineering and Ecology, Dushanbe, Republic of Tajikistan), ISASUZ (Institute of Seismology of the Academy
692 of Science of Uzbekistan, Tashkent, Uzbekistan), LLP (Institute of Seismology of the Science Committee of the
693 Republic of Kazakhstan, Almaty).

694 **Author contribution.** Ascanio Rosi implemented the landslide susceptibility model, William Frodella conceived
695 with Ascanio Rosi the article structure and collected the data, Nicola Nocentini prepared the landslide
696 susceptibility data and supported the model implementation, Francesco Caleca prepared the infrastructure data for
697 the model implementation and performed the statistical analysis involving the landslide susceptibility areas and
698 the exposed elements. All the above mentioned authors contributed to the writing of the article and the figure
699 graphics. Hans Balder Havenith and Alexander Strom provided the landslide databases from: i) Havenith, H.B.,
700 Strom, A., Torgoev, I., Torgoev, A., Lamair, L., Ischuk, A., Abdrakhmatov, K.: Tien Shan geohazards database:
701 Earthquakes and landslides. *Geomorphology* 249, 16–31, 2015a; and ii) Strom, A., Abdrakhmatov, K.: Rockslides
702 and rock avalanches of Central Asia: distribution, morphology, and internal structure. Elsevier, 441pg. ISBN: 978-

703 0-12-803204-6, 2018. They also provided the landslide pictures for figures 3 and 4, and critically reviewed the
704 paper. Veronica Tofani coordinated the work and reviewed the paper.

705 **Competing interests.** The contact author has declared that none of the authors has any competing interests.

706 **Acknowledgements.** This work was developed within World Bank-funded project “*Strengthening Financial*
707 *Resilience and Accelerating Risk Reduction in Central Asia*” (SFRARR), in collaboration with the European Union,
708 and the GFDRR (Global Facility for Disaster Reduction and Recovery), with the goal of improving financial
709 resilience and risk-informed investment planning in the central Asian countries (Kazakhstan, Kyrgyz Republic,
710 Tajikistan, Turkmenistan and Uzbekistan). This work represents the outcomes of the Task 7 “Landslide Scenario
711 Assessment”, coordinated by the UNESCO Chair on Prevention and Sustainable Management of Geo-
712 Hydrological Hazards (University of Florence). In particular, the authors would like to thank Gabriele Coccia and
713 Paola Ceresa from Red Risk Engineering (Pavia, Italy) for providing river network data and for the valuable
714 coordination and constant support, as well as Valerio Poggi and Chiara Scaini from OGS (National Institute of
715 Oceanography and Experimental Geophysics, Seismological Research Center, Trieste, Italy) for providing seismic
716 data (active faults, Pga) and exposure data. We would also like to thank the partners from Central Asia for the
717 fruitful collaboration, in particular: IWPHE (Tajikistan), ISASUZ (Uzbekistan) and LLP (Kazakhstan).

718 **References**

- 719 Abdrakhmatov, K. Y., Aldazhanov, S. A., Hager, B. H., Hamburger, M. W., Herring, T. A., Kalabaev, K. B.,
720 Makarov, P. Molnar, S. V. Panasyuk, M. T. Prilepin, R. E. Reilinger, I. S. Sadybakasov, B. J. Souter, Yu. A.
721 Trapeznikov, V. Ye. Tsurkov Zubovich, A. V. Relatively recent construction of the Tien Shan inferred from
722 GPS measurements of present-day crustal deformation rates. *Nature*, 384(6608), 450-45319, 1996.
- 723 Abdrakhmatov, K., Havenith, H.B., Delvaux, D., Jongmans, D., Trefois, P.: Probabilistic PGA and Arias Intensity
724 Maps of Kyrgyz Republic (Central Asia). *J. Seismol.* 7.2: 203-220, 2003.
- 725 Akgun, A. A.: comparison of landslide susceptibility maps produced by logistic regression, multi-criteria decision,
726 and likelihood ratio methods: A case study at İzmir, Turkey. *Landslides*, 9, 93–106, 2012.
- 727 Bazzurro, P. et al.: Strengthening Financial Resilience and Accelerating Risk Reduction in Central Asia - the
728 SFRARR project. The SFRARR probabilistic flood hazard assessment. In prep. for the Special Issue
729 “Regionally consistent risk assessment for earthquakes and floods and selective landslide scenario analysis
730 in Central Asia”. *Natural Hazards and Earth System Sciences (NHES)*.
- 731 Behling, R., Roessner, S., Kaufmann, H., Kleinschmit, B.: Automated spatiotemporal landslide mapping over large
732 areas using rapideye time series data. *Remote Sens.* 6, 8026–8055, 2014.
- 733 Behling, R., Roessner, S., Golovko, D., Kleinschmit, B.: Derivation of long-term spatiotemporal landslide
734 activity—A multi-sensor time series approach. *Remote Sens. Environ.* 186, 88–104, 2016.
- 735 Behling, R., Roessner, S.: Multi-temporal landslide inventory for a study area in Southern Kyrgyz Republic
736 derived from RapidEye satellite time series data (2009 – 2013). V. 1.0. GFZ Data Services.
737 <https://doi.org/10.5880/GFZ.1.4.2020.001>, 2020.

738 Brabb, E.E.: Innovative approaches to landslide hazard mapping, in: Proceedings 4th International Symposium on
739 Landslides, Toronto, 1, 307–324, 1984.

740 Breiman, L.: Random forests. *Mach. Learn.* 45, 5–32, 2001.

741 Brenning, A.: Spatial prediction models for landslide hazards: Review, comparison and evaluation. *Nat. Hazard*
742 *Earth Syst.* 5, 853–862, 2005.

743 CAC DRMI: Risk assessment for Central Asia and Caucasus: desk study review, 2009.

744 Carrara, A.: Multivariate models for landslide hazard evaluation. *J. Int. Assoc. Math. Geol.* 15, 403–426, 1983.

745 Cascini, L.: Applicability of landslide susceptibility and hazard zoning at different scales. *Eng. Geol.*, 102 (3-
746 4):164–177, 2008.

747 Catani, F., Lagomarsino, D., Segoni, S., Tofani, V.: Landslide susceptibility estimation by random forests
748 technique: sensitivity and scaling issues. *Nat. Hazards Earth Syst. Sci.* 13, 2815, 2013.

749 Chedia, O.K., Lemzin, I.N.: Seismogenerating faults of the Chatkal depression. In: *Seismotectonics and seismicity*
750 *of the Tien Shan.* Frunze, Ilim, 18–28, 1980.

751 Chen, L., Van Westen, C.J., Hussin, H., Ciurean, R.L., Turkington, T., Chavarro-Rincon, D., Shrestha, D.P.:
752 Integrating expert opinion with modelling for quantitative multi-hazard risk assessment in the Eastern Italian
753 Alps. *Geomorphology*, 273 (15):150–167, 2016.

754 Coccia, G. et al.: The SFRARR probabilistic flood hazard assessment. In prep. for the Special Issue “Regionally
755 consistent risk assessment for earthquakes and floods and selective landslide scenario analysis in Central
756 Asia”. *Natural Hazards and Earth System Sciences (NHES)*.

757 Corominas, J., Copons, R., Vilaplana, J.M., Altimir, J., Amigó, J.: Integrated landslide susceptibility analysis and
758 hazard assessment in the principality of Andorra. *Nat. Hazards*, 30 (3): 421–435, 2003.

759 Cruden, D.M., Varnes, D.J.: Landslide types and processes. *Landslides: Investigation and Mitigation. Special*
760 *Report 247, Transportation Research Board, Washington*, 36–75, 1996.

761 Danneels, G., Bourdeau, C., Torgoev, I., Havenith, H. B. Geophysical investigation and dynamic modelling of
762 unstable slopes: case-study of Kainama (Kyrgyzstan). *Geophysical Journal International*, 175(1), 17-34,
763 2008.

764 Delvaux, D., Abdrakhmatov, K.E., Lemzin, I.N., Strom, A.L.: Landslides and surface breaks of the 1911 Ms 8.2
765 Kemin earthquake, Kyrgyzstan, *Russian Geology and Geophysics*, 2001, 42, 10, 1667-1677, 2001.

766 Duman, T.Y., Can, T., Gokceoglu, C., Sonmez, H.: Application of logistic regression for landslide susceptibility
767 zoning of Cekmece Area, Istanbul, Turkey. *Environ. Geol.* 51, 241–256, 2006.

768 Ermini, L., Catani, F., Casagli, N.: Artificial Neural Networks applied to landslide susceptibility assessment.
769 *Geomorphology*, 66, 327–343, 2005.

770 European Commission Humanitarian Aid, Civil Protection, U.N.I.S. for D.R.R.: Disaster Risk Reduction 20

771 Examples of Good Practice from Central Asia, 2006.

772 Frattini, P., Crosta, G., Carrara, A.: Techniques for evaluating the performance of landslide susceptibility models.
773 Engineering geology, 111(1-4), 62-72, 2010.

774 GFDRR (Global Facility for Disaster Reduction and Recovery): Disaster Risk Management Notes for Priority
775 Countries 2009-2015. Eur. Asia 48–49, 2009.

776 GFDRR (Global Facility for Disaster Reduction and Recovery): Europe and Central Asia-Country Risk Profiles
777 for Floods and Earthquakes. 144 pg, 2016.

778 Goetz, J.N., Brenning, A., Petschkoc, H. Leopold P.: Evaluating machine learning and statistical prediction tech-
779 niques for landslide susceptibility modeling. Comput Geosci., 81, 1-11, 2015.

780 Golovko, D., Roessner, S., Behling, R., Wetzal, H. U., Kleinschmidt, B: Development of multi-temporal landslide
781 inventory information system for southern Kyrgyz Republic using GIS and satellite remote sensing. PFG
782 2015, 157–172, 2015.

783 Havenith, H. B., Strom, A., Jongmans, D., Abdrakhmatov, A., Delvaux, D., Tréfois, P.: Seismic triggering of
784 landslides, Part A: Field evidence from the Northern Tien Shan. Natural Hazards and Earth System Sciences,
785 3(1/2), 135-149, 2003.

786 Havenith, H.B., Strom, A., Cacerez, F., Pirard, E.: Analysis of landslide susceptibility in the Suusamyр region,
787 Tien Shan: statistical and geotechnical approach. Landslides 3, 39–50, 2006a.

788 Havenith, H.B., Torgoev, I., Meleshko, A., Alioshin, Y., Torgoev, A., Danneels, G.: Landslides in the Mailuu-Suu
789 Valley, Kyrgyz Republic—hazards and impacts. Landslides 3, 137–147, 2006b.

790 Havenith, H.B., Strom, A., Torgoev, I., Torgoev, A., Lamair, L., Ischuk, A., Abdrakhmatov, K.: Tien Shan
791 geohazards database: Earthquakes and landslides. Geomorphology 249, 16–31, 2015a.

792 Havenith, H.B., Torgoev, A., Schlögel, R., Braun, A., Torgoev, I., Ischuk, A.: Tien Shan geohazards database:
793 Landslide susceptibility analysis. Geomorphology 249, 32–43, 2015b.

794 Havenith, H.B., Torgoev, A., Braun, A., Schlögel, R., Micu, M.: A new classification of earthquake-induced
795 landslide event sizes based on seismotectonic, topographic, climatic and geologic factors. Geoenvironmental
796 Disasters, 1(3), 1-24, 2016.

797 Havenith, H.B., Umaraliev, R., Schlögel, R., Torgoev, I., Ruslan, U., Schlogel, R., Torgoev, I.: Past and Potential
798 Future Socioeconomic Impacts of Environmental Hazards in Kyrgyz Republic. In Kyrgyz Republic: Political,
799 Economic and Social Issues; Olivier, A.P., Ed.; Nova Science Publishers, Inc.: Hauppauge, NY, USA; pp.
800 63–113, 2017.

801 Hong, Y., Adler, R., Huffman, G.: Use of satellite remote sensing data in the mapping of global landslide
802 susceptibility. Nat. Hazards, 43, 23–44, 2007.

803 Ishihara, K., Okusa, S., Oyagi, N., Ischuk, A.: Liquefaction-induced flow slide in the collapsible loess deposit in
804 Soviet Tajik. Soils and foundations, 30(4), 73-89, 1990.

805 Juliev, M., Pulatov, A., Hubl, J.: Natural hazards in mountain regions of Uzbekistan: A review of mass movement
806 processes in Tashkent province. *International Journal of Scientific & Engineering Research*, 8(2), 1102,
807 2017.

808 Kalmetieva, Z.A., Mikolaichuk, A. V, Moldobekov, B.D., Meleshko, A. V, Janaev, M.M., Zubovich, A. V.: Atlas
809 of earthquakes in Kyrgyz Republic. Central-Asian Institute for Applied Geosciences and United Nations
810 International Strategy for Disaster Reduction Secretariat Office in Central Asia, Bishkek, p 75, 2009.

811 Kirschbaum, D., Stanley, T., Zhou, Y.: Spatial and temporal analysis of a global landslide catalog. *Geomorphology*,
812 249, 4-15, 2015.

813 Lagomarsino, D., Tofani, V., Segoni, S., Catani, F., Casagli, N.: A tool for classification and regression using
814 random forest methodology: Applications to landslide susceptibility mapping and soil thickness modeling.
815 *Environ. Model. Assess.*, 22, 201–214, 2017.

816 Lee, S.: Application of logistic regression model and its validation for landslide susceptibility mapping using GIS
817 and remote sensing data. *Int. J. Remote Sens.*, 26, 1477–1491, 2005.

818 Li, F., Torgoev, I., Zaredinov, D., Li, M., Talipov, B., Belousova, A., Kunze, C., Schneider, P.: Influence of
819 Earthquakes on Landslide Susceptibility in a Seismic Prone Catchment in Central Asia. *Appl. Sci*, 11, 3768,
820 2021.

821 Manzo, G., Tofani, V., Segoni, S., Battistini, A., Catani, F.: GIS techniques for regional-scale landslide
822 susceptibility assessment: The Sicily (Italy) case study. *Int. J. Geogr. Inf. Sci.*, 27, 1433–1452, 2013.

823 Martelloni, G., Segoni, S., Fanti, R., Catani, F.: Rainfall thresholds for the forecasting of landslide occurrence at
824 regional scale. *Landslides*, 9, 485-495, 2012.

825 Medeu, A.R., Blagovechshenskiy, A.R.: Seismogenic Landslide risk zoning in the surrounding areas of Almaty
826 city, Kazakhstan. *Vestnick*, 6, 121, 2016.

827 Molnar, P., Tapponnier, P.: Cenozoic Tectonics of Asia: Effects of a Continental Collision: Features of recent
828 continental tectonics in Asia can be interpreted as results of the India-Eurasia collision. *science*, 189(4201),
829 419-426, 1975.

830 Nadim, F., Kjekstad, O., Peduzzi, P., Herold, C., Jaedicke, C.: Global landslide and avalanche hotspots. *Landslides*,
831 3(2), 159-173, 2006.

832 Niyazov, R.A.: Landslides in Uzbekistan. FAN, Tashkent, 207 pp (in Russian), 2009.

833 Niyazov, R.A., Nurtaev, B.S.: Evaluation of Landslides in Uzebekistan Caused by the Joint Impact of Precipitation
834 and Deep-focus Pamir-Hindu Earthquakes. In *Landslides: Global Risk Preparedness* (pp. 253-265). Springer,
835 Berlin, Heidelberg, 2013.

836 Niyazov R.A.: Uzbekistan landslides. Uzbekistan landslide service. Technical report, 2020a.

837 Niyazov, R., Nurtaev, B., Bimurzaev, G., Tashpulatov, M.: Flow Slides in Uzbekistan: Overview and Case Studies.
838 In *Workshop on World Landslide Forum* (pp. 59-65). Springer, Cham, 2020b.

839 Pánek, T., Korup, O., Minár, J., Hradecký J.: Giant landslides and highstands of the Caspian Sea, *Geology*, 44
840 (11), 939–942, 2016.

841 Persits, F. M., Ulmishek, G. F., Steinshouer, D. W.: Maps showing geology, oil and gas fields and geologic
842 provinces of the Former Soviet Union (No. 97-470-E). US Geological Survey, 1997.

843 Piroton, V., Schlögel, R., Barbier, C., Havenith, H.B.: Monitoring the recent activity of landslides in the Mailuu-
844 suu valley (Kyrgyz Republic) using radar and optical remote sensing techniques. *Geosciences*, 10 (5), p. 164,
845 2020.

846 Pittore, M., Ozturk, U., Moldobekov, B., Saponaro, A.: EMCA Landslide catalog Central Asia. V. 1.0. GFZ Data
847 Services, 2018.

848 Poggi, V. et al. a.: Harmonising seismicity information in Central Asia: earthquake catalogue and faults. The
849 SFRARR probabilistic flood hazard assessment. In prep. for the Special Issue “Regionally consistent risk
850 assessment for earthquakes and floods and selective landslide scenario analysis in Central Asia”. *Natural
851 Hazards and Earth System Sciences (NHESS)*.

852 Poggi, V. et al. b.: Development of a state of art probabilistic seismic hazard model for Central Asia countries.
853 The SFRARR probabilistic flood hazard assessment. In prep. for the Special Issue “Regionally consistent
854 risk assessment for earthquakes and floods and selective landslide scenario analysis in Central Asia”. *Natural
855 Hazards and Earth System Sciences (NHESS)*.

856 Pollner, J., Kryspin-Watson, J., Nieuwejaar, S.: Disaster Risk Management and Climate Change Adaptation in
857 Europe and Central Asia. World Bank 1–53, 2010.

858 Pusch, C.: A comprehensive risk management framework for Europe and Central Asia. (No. 9). Disaster Risk
859 Management Working Paper Series, 2004.

860 Reichenbach, P., Rossi, M., Malamud, B.D., Mihir, M., Guzzetti, F.: A review of statistically-based landslide
861 susceptibility models. *Earth Sci. Rev.* 180, 60–91, 2018.

862 Roessner, S., Wetzel, H. U., Kaufmann, H., Kornus, W., Lehner, M., Reinartz, P., Mueller, R. Landslide
863 Investigations in Southern Kyrgyz Republic Based on a Digital Elevation Model Derived from MOMS-2P
864 Data. IAPRS, Vol. 33, Part B7, Amsterdam, pp. 1259 -1266, 2000.

865 Roessner, S., Wetzel, H.U., Kaufmann, H., Sarnagoev, A.: Satellite Remote Sensing and GIS Based Analysis of
866 Large Landslides in Southern Kyrgyz Republic NATO Advanced Research Workshop: Security of Natural
867 and Artificial Rockslide Dams”, Bishkek, Kyrgyz Republic 2004.

868 Roessner, S., Wetzel, H.U., Kaufmann, H., Sarnagoev, A.: Potential of Satellite Remote Sensing and GIS for
869 Landslide Hazard Assessment in Southern Kyrgyz Republic (Central Asia)”, *Natural Hazards*, Vol. 35, No.
870 3, pp. 395 -416, 2005.

871 Saponaro, A., Pilz, M., Wieland, M., Bindi, D., Moldobekov, B., Parolai, S., Landslide susceptibility analysis in
872 data-scarce regions: the case of Kyrgyz Republic. *Bull. Eng. Geol. Environ.* 74, 1117–1136, 2014.

873 Scaini, C. et al.: (in prep.) A new regionally consistent exposure database for Central Asia: population and
874 residential buildings. In prep. for the Special Issue “Regionally consistent risk assessment for earthquakes
875 and floods and selective landslide scenario analysis in Central Asia”. *Natural Hazards and Earth System
876 Sciences (NHESS)*.

877 Schiavina, M., Melchiorri, M., Pesaresi, M., Politis, P., Freire, S., Maffenini, L., Florio, P., Ehrlich, D., Goch, K.,
878 Tommasi, P., Kemper, T.: *GHSL Data Package*, Publications Office of the European Union, Luxembourg,
879 2022, ISBN 978-92-76-53071-8, JRC 129516, 2022.

880 Schlögel, R., Torgoev, I., De, Marneffe, C., Havenith, H.B.: Evidence of a changing size-frequency distribution
881 of landslides in the Kyrgyz Tien Shan, Central Asia. *Earth Surf Process Landf* 36(12), 1658– 1669, 2011.

882 Segoni, S., Tofani, V., Rosi, A., Catani, F. Casagli, N.: Combination of rainfall thresholds and susceptibility maps
883 for dynamic landslide hazardassessment at regional scale. *Front Earth Sci.*, 6 (85), 2018.

884 Stanley, T., Kirschbaum, D.B.: A heuristic approach to global landslide susceptibility mapping. *Nat. Hazards* 87,
885 145–164, 2017.

886 Sternberg R.: Damming a river: a changing perspective on altering nature. *Renewable Sustainable Energy Rev*
887 10:165–197, 2006.

888 Strom, A.L., Korup, O.: Extremely large rockslides and rock avalanches in the Tien Shan, Kyrgyz Republic.
889 *Landslides* 3, 125–136, 2006.

890 Strom, A.: Landslide dams in Central Asia region. *Journal of the Japan Landslide Society*, 47(6), 309-324, 2010.

891 Strom, A., Abdrakhmatov, K.: Large-Scale Rockslide Inventories: From the Kokomeren River Basin to the Entire
892 Central Asia Region (WCoE 2014–2017, IPL-106-2, in: *Workshop on World Landslide Forum*. Springer,
893 Cham, pp. 339–346, 2017.

894 Strom, A., Abdrakhmatov. K.: *Rockslides and rock avalanches of Central Asia: distribution, morphology, and
895 internal structure*. Elsevier, 441pg. ISBN: 978-0-12-803204-6, 2018.

896 Styron, R., Pagani, M.: The GEM Global Active Faults Database.” *Earthquake Spectra*, vol. 36, no. 1_suppl, Oct.
897 2020, pp. 160–180, 2020.

898 Tien Bui, D., Tuan, T. A., Klempe, H., Pradhan, B., Revhaug, I. Spatial prediction models for shallow landslide
899 hazards: a comparative assessment of the efficacy of support vector machines, artificial neural networks,
900 kernel logistic regression, and logistic model tree. *Landslides*, 13, 361-378, 2016.

901 Thurman, M.: *Natural Disaster Risks in Central Asia: A Synthesis*. UNDP BCPR, 2011.

902 Tiranti D., Nicolò G., Gaeta A. R.: Shallow landslides predisposing and triggering factors in developing a regional
903 early warning system. *Landslides* 16 (2): 235–251, 2019.

904 Trifonov, V.G., Makarov, V.I., Scobelev, S.F.: The Talas-Fergana active right-slip faults. *Ann Tectonicae* 6:224–
905 237, 1992.

906 Trigila, A., Frattini, P., Casagli, N., Catani, F., Crosta, G., Esposito, C., Spizzichino, D.: Landslide susceptibility

907 mapping at national scale: the Italian case study, in: *Landslide Science and Practice*. Springer, Berlin,
908 Heidelberg, pp. 287–295, 2013.

909 Ullah, S., Bindi, D., Pilz, M., Danciu, L., Weatherill, G., Zuccolo, E., . Anatoly Ischuk, A., Mikhailova, N.N.,
910 Abdрахmatov, K., Parolai, S. Probabilistic seismic hazard assessment for Central Asia. *Annals of*
911 *Geophysics*, 58(1), 2015.

912 UN ISDR.: Risk assessment for Central Asia and Caucasus: desk study review, CAC DRMI 2009, Risk
913 Management Working Paper Series No. 9. The World Bank, 2009.

914 World Bank: Natural Disaster Hotspots: Case Studies. Disaster Risk Management Series No. 6, 2006.

915 World Bank: Investigation and Analysis of Natural Hazard Impacts on Linear Infrastructure in Southern Kyrgyz
916 Republic Desk and Field Studies Report. Report 68669, 2008.

917 World Bank: The Global Landslide Hazard Map: Final Project Report. Appendix A., 2020.

918 Yaning, C.: Landslide-debris flow and its prevention in Kazakhstan. *Arid Land Geography*, 1992.

919 Yamazaki, D., Ikeshima, D., Tawatari, R., Yamaguchi, T., O'Loughlin, F., Neal, J. C., Sampson, C.C., Kanae, S.,
920 Bates, P.D.: A high-accuracy map of global terrain elevations. *Geophysical Research Letters*, 44(11), 5844-
921 5853, 2017.

922 Yilmaz, I.: Landslide susceptibility mapping using frequency ratio, logistic regression, artificial neural networks
923 and their comparison: a case study from Kat landslides (Tokat—Turkey). *Computers & Geosciences*, 35 (6):
924 1125-1138, 2009.

925 Zubovich, A. V., Wang, X. Q., Scherba, Y. G., Schelochkov, G. G., Reilinger, R., Reigber, C., Mosienko, O.,
926 Molnar, P., Michajljow, W., Makarov, V.I., Li, J., Kuzikov, S.I., Herring, T.A., Hamburger, M.W., Hager
927 B.H., Dang, Y., Bragin, V.D., Beisenbaev, R.: GPS velocity field for the Tien Shan and surrounding regions.
928 *Tectonics*, 29(6), 2010.

929